Cyclin A–Cdk1 regulates the origin firing program in mammalian cells

Yuko Katsuno[a], Ayumi Suzuki[a], Kazuto Sugimura[b], Katsuzumi Okumura[b], Doaa H. Zineldeen[a], Midori Shimada[a], Hiroyuki Niida[a], Takeshi Mizuno[c], Fumio Hanaoka[c,d], and Makoto Nakanishi[a,1]

[a]Department of Cell Biology, Graduate School of Medical Sciences, Nagoya City University, 1 Kawasumi, Mizuho-cho, Mizuho-ku, Nagoya 467-8601, Japan; [b]Laboratory of Molecular and Cellular Biology, Graduate School of Bioresources, Mie University, 1577 Kurimamachiya-cho, Tsu, Mie 514-8507, Japan; [c]Cellular Physiology Laboratory, RIKEN Discovery Research Institute, and Solution Oriented Research for Science and Technology, Science and Technology Corporation, Wako, Saitama 351-0198, Japan; and [d]Faculty of Science, Gakushuin University, Toshima, Tokyo 171-8588, Japan

Edited by Tak Wah Mak, University of Toronto, Toronto, Canada, and approved January 12, 2009 (received for review September 18, 2008)

Somatic mammalian cells possess well-established S-phase programs with specific regions of the genome replicated at precise times. The ATR–Chk1 pathway plays a central role in these programs, but the mechanism for how Chk1 regulates origin firing remains unknown. We demonstrate here the essential role of cyclin A2–Cdk1 in the regulation of late origin firing. Activity of cyclin A2–Cdk1 was hardly detected at the onset of S phase, but it was obvious at middle to late S phase under unperturbed condition. Chk1 depletion resulted in increased expression of Cdc25A, subsequent hyperactivation of cyclin A2–Cdk1, and abnormal replication at early S phase. Hence, the ectopic expression of cyclin A2–Cdk1AF (constitutively active mutant) fusion constructs resulted in abnormal origin firing, causing the premature appearance of DNA replication at late origins at early S phase. Intriguingly, inactivation of Cdk1 in temperature-sensitive Cdk1 mutant cell lines (FT210) resulted in a prolonged S phase and inefficient activation of late origin firing even at late S phase. Our results thus suggest that cyclin A2–Cdk1 is a key regulator of S-phase programs.

Chk1 | DNA replication | molecular combing | ATR protein | checkpoint

Duplication of the eukaryotic genome is regulated by multiple elements including initiation of DNA replication, rate of fork progression, stability of replication forks, and the origin firing program (1). Replication origins are fired in small groups that are activated together within individual replication factories and thus can be visualized as foci (2). Replication origins in a single replication factory are actually comprised of several candidate origins, most of which are not normally used through the mechanism by which firing of 1 origin inhibits activation of any other Mcm2–7 complexes within that factory (3). Thus, S-phase programs appear to be regulated by 2 distinct levels of origin firing; one is the sequential activation of replicon clusters characterized as visible replication foci, and the other is the selection of 1 Mcm2–7 complex around the ORC within a single replication factory.

The DNA replication checkpoint system was reported to be involved in the origin firing program in vertebrate cells (4). In analysis using *Xenopus* egg extract, ATR/Chk1 was shown to regulate the sequential activation of early and late replication origins (5). Chk1 also regulates the density of active replication origins during S phase of avian cells (6). Therefore, ATR/Chk1 may be involved in the regulation of sequential activation of replicon clusters and selection of origins within a single replication factory. Chk1 has been shown to regulate the physiological turnover of Cdc25A and its phosphatase activity, which in turn regulates several cyclin–Cdk activities (7) that are prerequisite for origin firing throughout S phase.

In budding yeast, Clb5-dependent Cdk activity is indispensable for activation of late replication origins (8), suggesting the existence of a specific transfactors for late origin activation in other eukaryotes. In fission yeast, however, clear late origins have not been characterized (9) and replication origins fire stochastically (10, 11). As for mammals, although almost half of origins are activated equally throughout S-phase progression (12), stable subunits of chromosomes equivalent to replication foci maintain their replication timing from S phase to S phase (13).

In this article, we demonstrate that Chk1 depletion resulted in an aberrant origin firing and a hyperactivation of cyclin A2–Cdk1 at early S phase. Ectopic expression of cyclin A2–Cdk1AF induced late origin firing at early S phase, and a loss of Cdk1 activity compromised activation of late origins at late S phase. Our results thus suggested that cyclin A2–Cdk1 might function as a transregulator of late origin firing in mammals.

Results

Chk1 Depletion Results in an Aberrant Origin Firing and a Hyperactivation of Cyclin A2–Cdk1 at Early S Phase. $Chk1^{lox/-}$ mouse embryonic fibroblasts (MEFs) were infected with adenoviruses expressing either LacZ or Cre and synchronized into G_0 phase by serum starvation (14). $Chk1^{lox/-}$ and $Chk1^{del/-}$ MEFs were then stimulated by 15% serum and double-labeled with iododeoxyuridine (IdU) and chlorodeoxyuridine (CIdU) at the indicated times, and their spatiotemporal patterns of replication sites were examined. The mammalian S phase is structured so that the sequential activation of replicon clusters occurs at spatially adjacent sites (15). This spatial relationship is maintained in $Chk1^{lox/-}$ MEFs (Fig. 1*A*), where 86.6 ± 4.4 of foci showed colocalization visualized as yellow color. In contrast, colocalization was detected only at 53.9 ± 4.8 of foci in $Chk1^{del/-}$ MEFs (Fig. 1*B*), indicating that Chk1 depletion in mammals resulted in the aberrant origin firing as observed in avian cells (6). Molecular combing of single DNA molecules was performed to visualize individual origin activation, measure the fork elongation, and define replication structures (Fig. 1*C* and Fig. S1). In asynchronized $Chk1^{lox/-}$ MEFs infected with control LacZ adenoviruses interorigin spacing (90.4 kb on average) was similar to that in mock-infected cells. Chk1 depletion resulted in a clear reduction in origin spacing (34.8 kb on average)(Fig. 1*C Top*). Spatiotemporal pattern of replication sites could also be affected by fork elongation. Chk1 depletion reduced the rate of fork elongation throughout the labeling period (Fig. 1*C Middle*).

Double-labeling protocol also defines 5 classes of replication structure as described (6). Chk1 depletion resulted in a significant reduction in a proportion of consecutively elongating forks (class 1) and an increase in number of new firing initiation during the first (class 2) and second (class 4) labeling period (Fig. 1*C Bottom*). A dramatic increase in the frequency of closely-spaced active origins

Author contributions: M.N. designed research; Y.K., A.S., K.S., K.O., D.H.Z., M.S., and H.N. performed research; T.M. and F.H. contributed new reagents/analytic tools; Y.K., K.S., and M.N. analyzed data; and Y.K. and M.N. wrote the paper.

The authors declare no conflict of interest.

This article is a PNAS Direct Submission.

[1]To whom correspondence should be addressed. E-mail: mkt-naka@med.nagoya-cu.ac.jp.

This article contains supporting information online at www.pnas.org/cgi/content/full/0809350106/DCSupplemental.

www.pnas.org/cgi/doi/10.1073/pnas.0809350106

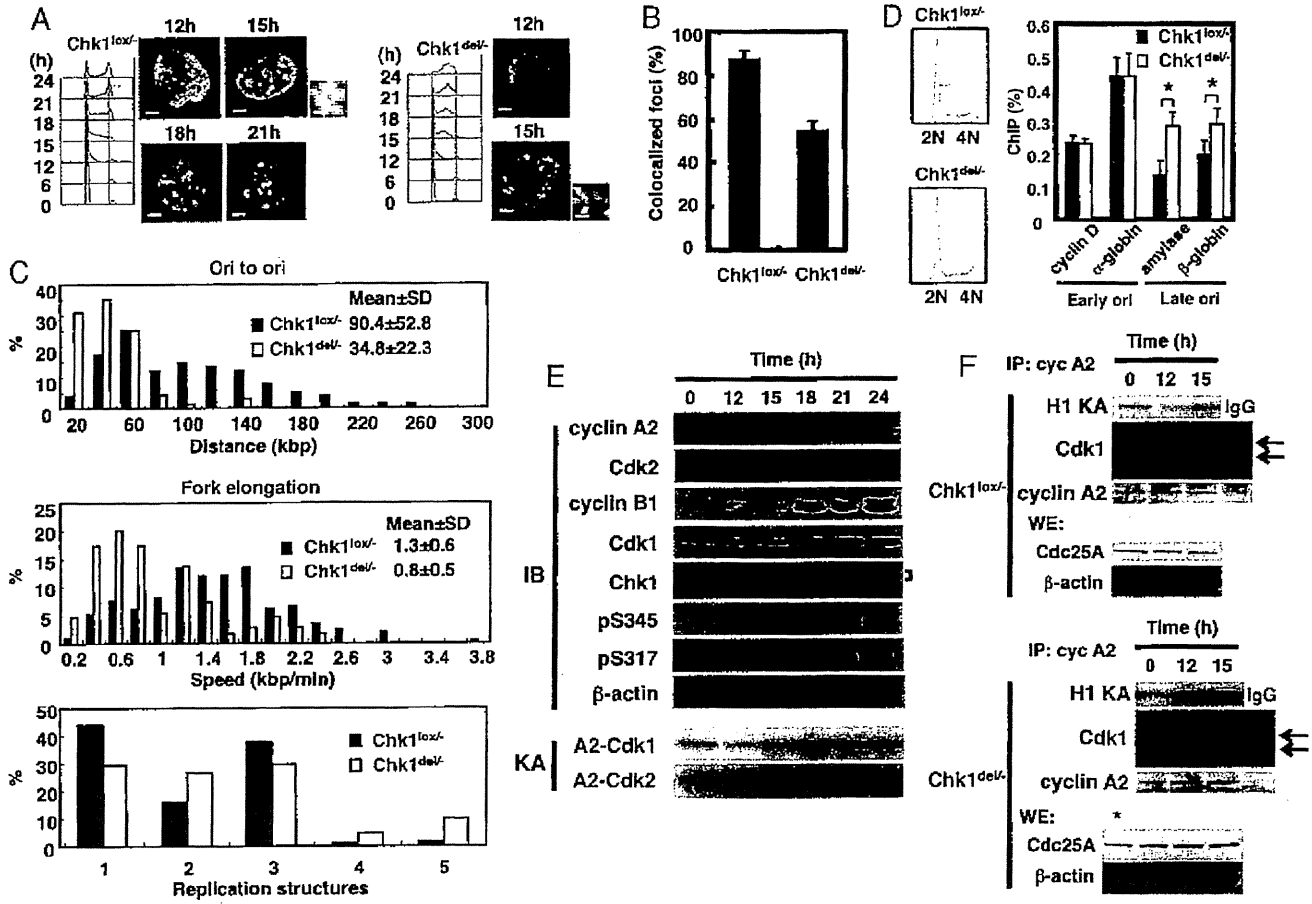

Fig. 1. Chk1 depletion results in an aberrant S-phase program and an activation of cyclin A2–Cdk1 at early S phase. (*A*) Chk1$^{lox/-}$ and Chk1$^{del/-}$ MEFs were synchronized at quiescence by serum starvation and then released by the addition of 15% serum. Cells were harvested at the indicated times, and their cell cycle distributions were analyzed by FACS. Replication sites were pulse-labeled for 15 min with 100 μM IdU and then for 15 min with 100 μM CldU, and analyzed with a Zeiss LSM5 confocal fluorescence microscope. Typical patterns of replication sites at the indicated times are presented. High-power details are from the boxed areas shown. (Scale bars: 5 and 0.5 μm in detail.) (*B*) Colocalization of IdU and CldU foci in Chk1$^{lox/-}$ and Chk1$^{del/-}$ MEFs. Relative colocalization of IdU and CldU foci was determined as a percentage of total foci in both cells ($n > 30$). Data are means ± SD of at least 3 independent experiments. (*C*) Asynchronized Chk1$^{lox/-}$ MEFs were infected with the indicated adenoviruses and double-labeled with IdU and CldU before harvesting at 28 h after infection. Replication structures were visualized by means of dynamic molecular combing. Adjacent origins in replicon clusters (Ori to ori), fork elongation, and replication structure defined by ref. 6 were determined ($n > 100$). Frequency histograms show the distribution of separation in distance (kbp), speed (kbp/min), and replication structure (1, elongating fork; 2, fork growing from 1 ori; 3, terminal fusions; 4, isolated; 5, interspersed). (*D*) Asynchronized Chk1$^{lox/-}$ MEFs were infected with adenoviruses expressing either LacZ or Cre. Cells were labeled with BrdU for 1 h before harvesting at 28 h after infection, and the cell cycle profiles were then analyzed by FACS. Early S-phase fraction indicated by bars was sorted, and nascent DNA was enriched by immunoprecipitation using α-BrdU. The indicated genes were amplified by quantitative PCR, and the results are presented as a percentage of mtDNA. Data are means ± SD of at least 3 independent experiments. Statistical significance was assessed by Student's *t* test (*, $P < 0.01$). (*E*) Synchronized Chk1$^{lox/-}$ MEFs as in *A* were harvested at the indicated times, and the lysates were subjected to immunoblotting by using the indicated antibodies or to an in vitro kinase assay (KA) for cyclin A2–Cdk1 and cyclin A2–Cdk2 with HH1 (2 μg) as a substrate. (*F*) Synchronized Chk1$^{lox/-}$ and Chk1$^{del/-}$ MEFs as in *A* were harvested at the indicated times, and the lysates were immunoprecipitated by using α-cyclin A2 antibodies after 3 times preabsorbance with α-Cdk2. The resultant immunoprecipitates (IP: cyclin A2) or whole-cell extracts (WE) were subjected to immunoblotting or in vitro kinase assay as in *E*. Arrows indicate the fast (active) or slow (inactive) migrated bands of Cdk1. An asterisk represents cell lysates from Chk1$^{lox/-}$ MEFs at 15 h.

(class 5) was observed. These observations suggest that loss of Chk1 frequently stalls and collapses active forks.

We next examined whether Chk1 regulates global sites of DNA synthesis by quantitative ChIP using FACS-based cell sorting (16). To avoid unexpected effects from gross changes in cell cycle profile on this analysis, we analyzed Chk1$^{del/-}$ MEFs 28 h after adenoviral infection, the time at which Chk1 was completely depleted, but the cell cycle profile was almost the same as that of Chk1$^{lox/-}$ cells (Fig. 1*D*). Cells from the first third of S phase were collected (Fig. 1*D Left*). Nascent (BrdU-containing) DNA was enriched by immunoprecipitation using α-BrdU antibodies and amplified by quantitative PCR with specific primers for cyclin D and α-globin for early-replicating DNA and primers for amylase and β-globin for late-replicating DNA. We also monitored amplification of mtDNA as a control, which replicates throughout the cell cycle and is equally represented in nascent DNA preparations (16, 17). The relative amounts of early replication (cyclin D and α-globin) in Chk1$^{del/-}$ MEFs were almost the same as those in Chk1$^{lox/-}$ cells, whereas those of late replication (amylase and β-globin) in Chk1$^{del/-}$ MEFs were significantly higher than those in Chk1$^{lox/-}$ cells (Fig. 1*D Right*). Given that 1 cell possesses ≈1,000 copies of mitochondrial genome, but they replicate throughout the cell cycle, relative amplification of nascent DNA (≈0.3) for early and late origins appeared consistent.

Chk1 is phosphorylated during unperturbed S phase (18, 19), which regulates the activity and stability of Cdc25 phosphatases, leading to the inactivation of Cdks through increased phosphorylation of their Y15 residues (20). Thus, we speculated that Chk1

regulates origin firing program through affecting certain cyclin–Cdks activities. The band corresponding to Chk1 was shifted upward at 15 h and thereafter. This band shift was reversed by phosphatase treatment, indicating that the modification was caused by phosphorylation. Chk1 phosphorylation was also confirmed by using phospho-specific antibodies to Chk1 at Ser-317 and Ser-345 (Fig. 1*E*).

Cyclin A2–Cdk1 activity was first detected at 15 h (middle S phase) and increases thereafter. Cyclin A2–Cdk2 was detected at 6 h (early S phase) and reached maximum at 18 h (Fig. 1*E* and Fig. S2*A*). These results are consistent with the recent report that cyclin A2 starts to form a complex with Cdk1 at mid-S phase (21). Cyclin A2–Cdk1 activity was detected earlier and enhanced in $Chk1^{del/-}$ MEFs when compared with $Chk1^{lox/-}$ MEFs (Fig. 1*F*), where immunodepletion of Cdk2 was equally achieved in both cyclin A2 immunoprecipitates (Fig. S2*B*). Cyclin A2–Cdk2 activity was not apparently affected by Chk1 depletion (Fig. S2*A*). Intriguingly, the amount of Cdc25A was highly elevated in $Chk1^{del/-}$ MEFs. Consistent with this increase in amount of Cdc25A, fast mobility band (active; Y15 dephosphorylation) and slow band (inactive; Y15 phosphorylation) of Cdk1 protein were dominant in those from $Chk1^{del/-}$ MEFs and $Chk1^{lox/-}$ MEFs, respectively (Fig. 1*F*). Specificity of cyclin A2–Cdk1 activity was confirmed by Cdk1 knockdown experiment, where cyclin A2–Cdk1 activities in both MEFs were significantly reduced after Cdk1 depletion (Fig. S3). To further confirm the functional interaction between Chk1 and cyclin A2–Cdk1, $Chk1^{lox/-}$ MEFs were treated with UV light, which phosphorylated Chk1 in an ATR-dependent manner. Chk1 phosphorylation was correlated with the reduction of Cdc25A, the appearance of slow mobility band of Cdk1 protein, and inhibition of cyclin A2–Cdk1 activity (Fig. S4). Taken together, cyclin A2–Cdk1 is likely to be a target of Chk1 through regulation of Cdc25A.

Aberrant Origin Firing in Cells Expressing Cyclin A2–Cdk1AF Fusion Protein. To examine the role of each cyclin–Cdk complex in the origin firing program, we generated a cyclin A2–Cdk1 fusion construct. Because cyclin–Cdk activities are regulated mainly by the phosphorylation of Y15, we generated a constitutively active mutant (CdkAF) in which residues at inhibitory phosphorylation sites were replaced with alanine and phenylalanine and therefore the mutant was not affected by the Chk1–Cdc25 pathway. Recombinant cyclin A2–Cdk2AF, cyclin A2–Cdk1AF, and cyclin B1–Cdk1AF complexes and the fusion proteins were examined for their enzymatic kinetics by using histone H1 (HH1) and lamin B as substrates. Dose-dependent increases in activities of both cyclin–Cdks complex and their fusion proteins were observed (Fig. 2*A*). The kinetic values of these complexes were the same as those of the fusion proteins (Table S1).

Expression of cyclin B1–Cdk1AF, but not cyclin A2–Cdk2AF or cyclin A2–Cdk1AF, induced γH2AX foci in HeLa cells (Fig. 2*B*). Amounts of cyclin B1–Cdk1AF, cyclin A2–Cdk1, and cyclin A2–Cdk2 fusion proteins expressed at 24 h after infection were almost equal to endogenous Cdk1 and Cdk2 proteins, respectively (Fig. 2*C* and Fig. S5). Again, γH2AX was not detected by immunoblotting in cells expressing cyclin A2–Cdk1 or cyclin A2–Cdk2 fusion protein.

Expression of cyclin A2–Cdk1AF and cyclin A2–Cdk2AF fusion protein at the endogenous level did not appear to affect the gross progression of S phase (Fig. 3*A*) although they arrested the cell cycle at M phase because of their inability to be degraded by APC-C at mitosis and thus mitotic exit was inhibited. The expression of cyclin A2–Cdk1AF fusion protein caused the appearance of late replication sites during early S phase when cells were double-labeled with IdU and CIdU (Fig. 3*B*). Dynamic molecular combing revealed that expression of cyclin A2–Cdk1AF fusion protein reduced origin spacing (75.0 kb on average), whereas that of cyclin A2–Cdk2AF

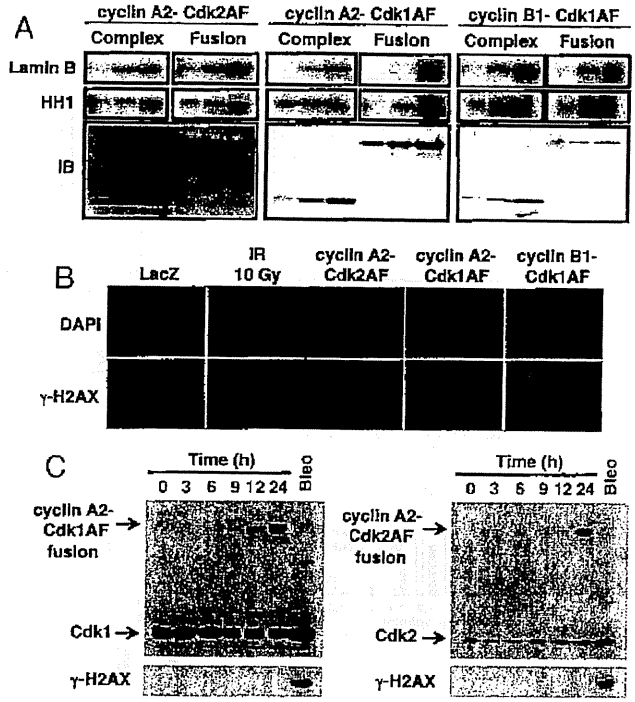

Fig. 2. Enzymatic kinetics of cyclin–Cdk fusion proteins. (*A*) Baculoviruses expressing cyclin A2 together with those expressing Cdk2 or Cdk1 (Complex) or those expressing cyclin A2–Cdk2, cyclin A2–Cdk1, or cyclin B1–Cdk1 fusion protein (Fusion) were used to infect insect cells. Their complexes or fusion proteins were purified and subjected to an in vitro kinase assay using lamin B (2 μg) or HH1 (2 μg) as a substrate or subjected to immunoblotting by using Cdk2 or Cdk1 antibodies (IB). (*B*) HeLa cells were infected with adenoviruses expressing the indicated proteins 24 h before fixing and immunostained with α-γH2AX antibodies. Their nuclei were counterstained with DAPI. As a positive control, cells infected with adenoviruses expressing LacZ were treated with IR (10 Gy). (Magnifications: 100×.) (*C*) HeLa cells were infected with adenoviruses expressing either cyclin A2-Cdk1AF or cyclin A2-Cdk2AF fusion proteins. Cells were harvested at the indicated times, and the lysates were subjected to immunoblotting using α-Cdk1 (*Upper Left*), α-Cdk2 (*Upper Right*), or α-γH2AX antibodies (*Lower*). As a control, HeLa cells were treated with bleomycin for 24 h (20 μg/mL).

did not (113.0 kb on average)(Fig. 3*C Top* and Fig. S6). Unlike Chk1 depletion, expression of cyclin A2–Cdk2AF did not cause significant changes in the proportion of abnormal replication structures (Fig. 3*C Bottom*). Taken together, these results suggested that cyclin A2–Cdk1 had a specific role in the origin firing program.

ChIP analysis revealed that considerable enrichment of early- and late-replicating DNA was specifically observed in the early and late S-phase fractions of control LacZ cells, respectively (Fig. 3*D*). Ectopic expression of cyclin A2–Cdk1AF resulted in the dramatic increase in replication of late origins in early S-phase fractions, but that of cyclin A2–Cdk2AF did not apparently affect it.

Cdk1 Is Required for Proper Timing of Origin Firing. FT210 cells possess a temperature-sensitive Cdk1 gene product (22). FACS analysis revealed a 2-h-longer S phase in FT210 cells compared with the parental FM3A cells (Fig. 4*A*). S-phase progression of FT210 cells at a permissive temperature was almost the same as that of FM3A cells. The progression of the spatiotemporal pattern of DNA replication sites in FM3A at the nonpermissive temperature was almost the same as in HeLa cells or MEFs. In contrast, the specific pattern of DNA replication sites observed in late S phase showing a few large internal foci was hardly detected in FT210 cells even at late S phase at nonpermissive temperature (Fig. 4*A*). Loss of Cdk1

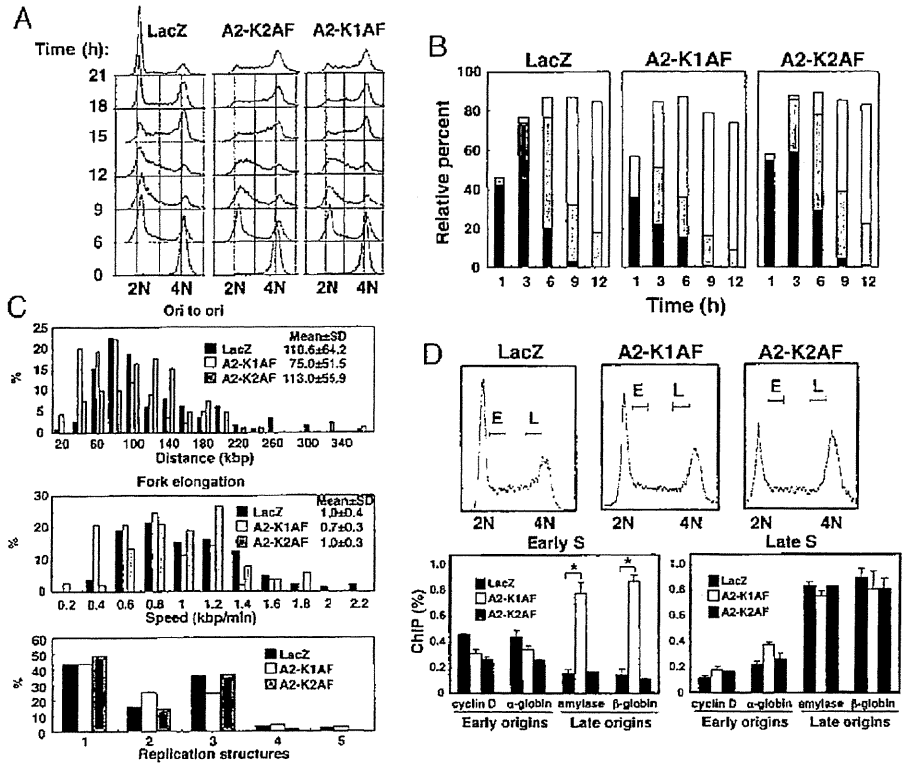

Fig. 3. Ectopic expression of cyclin A2-Cdk1AF, but not cyclin A2–Cdk2AF resulted in an aberrant temporal regulation of origin firing. (*A*) HeLa cells were synchronized by thymidine (2 mM, 24 h)/release period (6 h)/nocodazole (0.1 μg/mL, 12 h) and infected with adenoviruses expressing either cyclin A2–Cdk2AF, cyclin A2–Cdk1AF, or LacZ (control) 12 h before nocodazole washout (time 0). Cells were harvested at the indicated times, and their cell cycle profiles were analyzed by FACS. (*B*) HeLa cells were infected with the indicated adenoviruses 24 h before mimosine (0.6 mM, 16 h) washout (time 0). Replication sites were pulse-labeled for 15 min with IdU (100 μM) and then for 15 min with CldU (100 μM) before harvesting at the indicated times. The number of replication sites of each pattern was counted, and the relative percentage of the total number of cells ($n > 300$) is indicated. Black bars represent the early pattern, gray bars represent the middle pattern, and white bars represent the late pattern. Data are means of at least 3 independent experiments. (*C*) Asynchronous HeLa cells were infected with the indicated adenoviruses. Cells were harvested 24 h after infection and subjected to molecular combing. Adjacent origins in replicon clusters (Ori to ori), fork elongation, and replication structure were determined ($n > 100$) as in Fig. 1*C*. (*D*) Asynchronous HeLa cells infected with the indicated adenoviruses were pulse-labeled with BrdU before harvesting cells 24 h after infection. S-phase cells were then sorted into early (E) or late (L) fractions (*Upper*). The sorted cells were collected, and replication firing at the indicated origins was analyzed by ChIP analysis (*Lower*) as in Fig. 1*D*. Data are means ± SD of at least 3 independent experiments. Statistical significance was assessed by Student's *t* test (*, $P < 0.01$).

resulted in a significant increase in origin spacing (104.7 kb on average) when compared with control cells (78.6 kb on average) (Fig. 4*B Top* and Fig. S6). Loss of Cdk1 did not cause changes in the proportion of replication structures, further supporting the notion that Cdk1 is not involved in the stabilization of replication forks.

ChIP analysis revealed that replication patterns of early S-phase fractions in both cells were very similar, whereas replication of late origins in late S-phase fraction from FT210 cells was specifically impaired (Fig. 5*A Right*). Cdk2 activity during S phase in FT210 cells appeared the same as that in FM3A cells (Fig. S7). Collectively, these results suggested that Cdk1 activity is involved in the proper timing of late origin firing.

Finally, we attempted to determine the molecular basis by which cyclin A2–Cdk1 regulates origin firing program. In *Xenopus* and yeast systems, it was reported that cyclins, Cdk1 specifically, interact with the origin recognition complexes (ORCs) (23, 24). To examine whether the specific interaction of Cdk1 to ORCs is conserved among mammals, we performed ChIP analysis with α-Cdk1 and α-Cdk2 antibodies. Both Cdk1 and Cdk2 were detected at genes replicating early, whereas Cdk1 was specifically detected at genes replicating late (Fig. 5*B*). Relative binding of Cdk1 and Cdk2 appeared somewhat low, presumably because of an asynchronous cell cycle. These results suggested that the specific binding of Cdk1 to late origins may also be involved in the regulation of origin firing programs.

Discussion

Conditional Chk1 knockout MEFs revealed that Chk1 plays an important role in the regulation of origin firing at 2 distinct levels in mammals, namely activation of origins within a single replication factory and activation of replicon clusters (Fig. 1 *A–D*). Consistent with our observations, it was very recently proposed that Chk1 suppresses initiation in both inactive, later-firing clusters and active clusters, and the former is more strongly repressed (25). We then successfully showed that expression of cyclinA2–Cdk1AF fusion proteins activated origin firing at both levels as Chk1 depletion did (Fig. 3 *B–D*). The expression patterns of Cdk1 and cyclins during S phase and the enhancement of their activities in response to Chk1 depletion are also consistent with our conclusions (Fig. 1 *E* and *F*). The most striking evidence for the involvement of Cdk1 in DNA replication is the fact that inactivation of Cdk1 in mammalian cells resulted in a prolonged S phase accompanied by ineffective firing of late replicon clusters and reduced the density of active origins (Figs. 4 and 5*A*). Although our present results clearly demonstrate that cyclin A2–Cdk1 is involved in the regulation of late origin firing, functioning downstream of Chk1, we cannot rule out the possibility that cyclin A2–Cdk2 has a redundant function. Hochegger *et al.* (26) reported that Cdk1 activity was essential for DNA replication initiation when Cdk2 was depleted in chicken DT40 cells. When Cdk2 was present, Cdk1 inhibition did not delay S phase or block centrosome duplication. In this regard, DNA replication in DT40 cells appears complete within a shorter period (8 h) when compared with mammalian cells (10 h at 37 °C). Therefore, it is possible that DT40 cells possess a strong Cdk2 activity, presumably because of a loss of functional p53 that reduces the level of p21 Cdk inhibitor, and the high Cdk2 activity may compensate for the loss of Cdk1 activity in the context of S-phase control. In agreement with this notion, both Cdk1 and Cdk2 were recently reported to be involved in the control of DNA replication and replication origin firing under unperturbed S phase in the *Xenopus* system (27). It was also suggested that Cdk1 and Cdk2 must have different activities toward the genuine substrates involved in DNA replication although one kinase alone is minimally sufficient to promote substantial DNA replication.

Neither cyclin A2–Cdk1 nor cyclin A2–Cdk2 appeared to be involved in the stabilization of replication forks during S phase

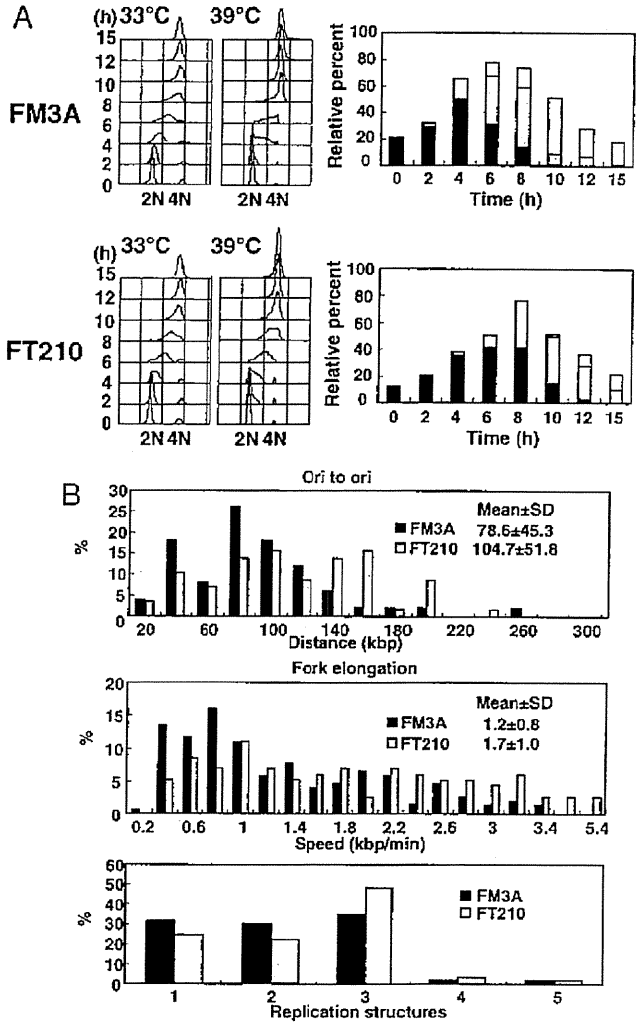

Fig. 4. Prolonged S phase in temperature-sensitive Cdk1 mutant FT210 cells. (*A*) FT210 and the parental FM3A cells were synchronized at M phase by nocodazole (0.5 μg/mL, 16 h) and then released at an either permissive (33 °C) or nonpermissive (39 °C) temperatures. Cells were then harvested 3 h after release (time 0) and at various times thereafter. Their replication sites were analyzed ($n > 300$) as in Fig. 3*B*. Data are means of at least 3 independent experiments. (*B*) Asynchronized FM3A and FT210 cells were shifted at 39 °C for 4 h. Cells were then harvested and subjected to molecular combing. Adjacent origins in replicon clusters (Ori to ori), fork elongation, and replication structure were determined ($n > 100$) as in Fig. 1*C*.

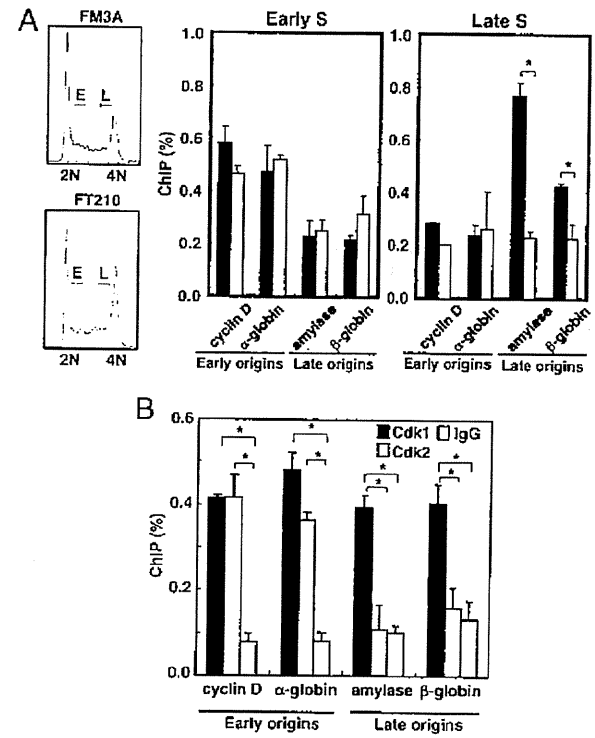

Fig. 5. Impaired late origin firing in temperature-sensitive Cdk1 mutant FT210 cells. (*A*) Asynchronous FM3A and FT210 cells were shifted at 39 °C for 4 h. Cells were pulse-labeled with BrdU (25 μM) for 1 h and sorted into early (E) or late (L) fractions. Replication firing at the indicated origins was analyzed by ChIP analysis as in Fig. 3*D*. Data are means ± SD of at least 3 independent experiments. Statistical significance was assessed by Student's *t* test (*, $P < 0.01$). Filled bars indicate FM3A cells; empty bars indicate FT210 cells. (*B*) Asynchronous FM3A cells were cultured at 33 °C and harvested. Cell lysates were subjected to ChIP analysis as described in *Materials and Methods*. Data are means ± SD of at least 3 independent experiments. Statistical significance was assessed by Student's *t* test (*, $P < 0.01$).

when replication structures were assessed by dynamic molecular combing technology (Fig. 3*C*). This idea was further supported by the observations that ectopic expression of cyclin A2–Cdk1AF and cyclin A2–Cdk2AF failed to induce DNA damage (Fig. 2 *B* and *C*). These findings present a clear contrast to the case with Chk1 depletion in which stability of replication forks during S phase was strikingly reduced. Therefore, Chk1 likely regulates the fork stability in a manner independent of cyclin–Cdk activities.

Cdk activities have both positive and negative roles during S phase, namely to initiate DNA synthesis and prevent rereplication. A quantitative model has proposed for explain the biphasic effects of Cdks (28). In addition to a quantitative model, the accessibility of Cdk to substrates could play a role in the regulation of the S-phase program. Studies in *Xenopus* and yeast systems suggested that Cdk1 specifically interacts with ORC and phosphorylates the components more efficiently than Cdk2 although this interaction is proposed to be involved in prevention of rereplication (23, 24). We found that Cdk1 could bind to both early and late origins but Cdk2 failed to bind to late origins (Fig. 5*B*). Thus, Cdk1 could potentially activate early origin firing. This notion is supported by the fact that Cdk1 could complement the Cdk2 function of S-phase initiation in Cdk2-depleted cells (26). However, because neither ectopic expression of cyclin A2–Cdk2AF nor cyclin A2–Cdk1AF resulted in the further enhancement of early origin activation (Fig. 3*D*), activation of endogenous cyclin A/E–Cdk2 at the S-phase onset appeared to be sufficient for early origin firing. Furthermore, given that the majority of endogenous Cdk1 and Cdk2 existed in soluble fractions (Fig. S8), the origin activation program appeared to be regulated not only by induction of Cdks and their binding to prereplicative complex components, but also by alternative ways such as complex formation with cyclins or regulation of inhibitory phosphorylation of Cdks. In this regard, it was very recently reported that Cdk1 started to form a complex with cyclin A2 after cyclin A2–Cdk2 complexes reached a plateau in mid S phase (21). Taken together, our results suggest that cyclin A2–Cdk1 may regulate origin firing program through both its specific accessibility to late origins and regulation of Cdk1 activity at late S phase.

In conclusion, the present results indicate that ATR/Chk1–cyclin A2–Cdk1 controls the activation of late replication origins and the density of active origins in mammals. Similar regulation was reported in a budding yeast system in which Clb5–Cdk1 was required for late origin firing (8). Taken together, these results suggest the existence of conserved mechanisms for the temporal program of origin activation among a number of eukaryotes.

Materials and Methods

Antibodies. Antibodies used in this study were as follows: α-CDK2 (sc-748; Santa Cruz), α-Cyclin A2 (sc-751; Santa Cruz), α-Cdc2 (sc-54; Santa Cruz), α-Cyclin B1 (sc-245; Santa Cruz), rat α-BrdU (ab6326; Abcam), mouse α-BrdU (347580; BD), α-γH2AX (05-636; Upstate), α-rabbit IgG HRP (NA934; GE Healthcare), α-mouse IgG HRP (NA931; GE Healthcare), Alexa Fluor 555-conjugated goat α-mouse IgG (A-21422; Invitrogen), and Alexa Fluor 488-conjugated rabbit α-rat IgG (A-21210; Invitrogen).

Cell Culture and Double Labeling with IdU and CldU. HeLa cells, $Chk1^{lox/-}$ MEFs, $Chk1^{del/-}$ MEFs, FM3A, and FT210 cells were cultured as described (14, 29). For analyses of origin firing programs, cells were incubated with 100 μM IdU for 15 min, then 100 μM CldU for 15 min, fixed with 4% paraformaldehyde, and permabilized. Cellular DNA was denatured in 1.5 M HCl and stained as reported (6). The spatiotemporal patterns of replication were analyzed by counting at least 300 cells by 2 individuals under blinded conditions.

Dynamic Molecular Combing and Immunofluorescent Detection. Genomic DNA was prepared and combed onto the silanated cover slips as described (30) with modifications as detailed (31). A total of 2×10^6 cells were pulse-labeled for 20 min with 100 μM IdU, washed with PBS twice, and pulse-labeled for 20 min with 100 μM CldU. For preparation of genomic DNA, to remove the mitochondrial genome the nuclei were extracted with buffer A [250 mM sucrose, 20 mM Hepes (pH 7.5), 10 mM KCl, 1.5 mM $MgCl_2$, 1 mM EDTA (pH 8.0), 1 mM EGTA (pH 6.8), 1 mM DTT, 0.1 mM PMSF] before resuspension into low-melting point agarose. Combed DNA molecules were heat-denatured in 50% formamide, 2 × SSC at 72 °C for 12 min. For immunodetection of labeled DNA, denatured DNA molecules were incubated with mouse α-BrdU mAb (1:5) and rat α-BrdU mAb (1:25) for 1 h at 37°C. After washing with PBS and 0.05% Tween 20 for 5 min 3 times, DNA molecules were incubated with Alexa Fluor 555-conjugated goat α-mouse IgG (1:500) and Alexa Fluor 488-conjugated rabbit α-rat IgG (1:500) for 30 min at 37°C. All antibodies were diluted in blocking solution [1% (wt/vol) blocking reagent in PBS, 0.05% Tween 20]. After washing with PBS and 0.05% Tween 20 for 5 min 3 times, coverslips were mounted in VECTASHIELD (Vector Laboratories). To estimate the extension of DNA molecules, coverslips were prepared with λ-DNA, and then the DNA molecules were stained with 6.7 mM YOYO-1 at 25°C for 1 h. YOYO-1-stained DNA molecules measured 21 ± 0.9 μm. As the virus genome is 48.5 kbp, the extension of DNA molecules is 2.32 ± 0.11 kbp/μm. DNA fibers were examined with a Zeiss Axioplan 2 MOT with a 63X Plan-APOCHROMAT (NA 1.4) objective lens, equipped with MicroMAX CCD camera (Princeton Instruments). Fluorescent signals were measured by using MetaMorph version 6.1 software (Universal Imaging).

Construction of Cyclin A2–Cdk1, Cyclin A2–Cdk2, and Cyclin B1–Cdk1 Fusion Vectors. For subcloning of full-length mouse Cdk1 and Cdk1AF, either cDNAs from mouse MEFs or pcDNA3.1Cdk1AF were used as a template. The PCR products were digested with EcoRI and NotI and subcloned into pcDNA3.1Myc/HisA vector (Invitrogen). For subcloning of full-length mouse Cdk2 and Cdk2AF, either cDNAs from mouse MEFs or pcDNA3.1Cdk2AF were used as a template. For preparation of cyclin A2–Cdk1, cyclin A2–Cdk2, and cyclin B1–Cdk1 fusion constructs, sets of primers and mouse cDNA derived from MEFs as a template were used. The PCR products were digested with BamHI and EcoRI and subcloned into pcDNA3.1Cdk1Myc/HisA or pcDNA3.1Cdk2Myc/HisA vectors. The primer sets used are listed in Table S1.

Purification of Recombinant Cyclin–Cdk Fusion Proteins. pcDNA3.1cyclin A2–Cdk1, pcDNA3.1cyclin A2–Cdk2, pcDNA3.1cyclin B1–Cdk1, and their AF mutants were digested with BamHI and PmeI. The fragments were subcloned into pVL1392 vector and transfected into Sf9 cells. Sf9 cells infected with baculoviruses expressing cyclin–Cdk fusion proteins or coinfected with the individual cyclins and Cdks were lysed with immunoprecipitation kinase buffer (7) containing a mixture of protease inhibitors. The fusion proteins and cyclin–Cdk complexes were purified by ProBond Resin (Invitrogen) and used for the in vitro kinase assay.

Preparation of Adenoviruses Expressing Cyclin–Cdk Fusion Proteins. The BamHI–PmeI fragments of cyclin–Cdk fusion constructs were subcloned into pENTER vector (Invitrogen) predigested with BamHI and EcoRV. pENTERcyclin–Cdks and pENTERcyclin–CdkAFs were then subcloned into pAdCMV vectors according to the manufacturer's instructions (Invitrogen). pAdcyclin–Cdks and pAdcyclin–CdkAFs were transfected into 293A cells (Invitrogen).

ChIP Assay. Asynchronized $Chk1^{lox/-}$ MEFs, $Chk1^{del/-}$ MEFs, HeLa cells infected with adenoviruses expressing cyclin A2–Cdk1AF or cyclin A2–Cdk2AF, and mouse FM3A or FT210 cells were labeled with 25 μM BrdU before cell sorting. Cells were then sorted into early and late S-phase fractions by using a cell sorter (BD). At least 60,000 cells were collected during each phase and used for the chromatin preparation. Nascent DNA was enriched by immunoprecipitation using α-BrdU antibodies as reported (16) and subjected to quantitative PCR with the ABI PRISM 7000 system using Power SYBR Green PCR Master Mix (Applied Biosystems). Primers used for PCR are listed in Table S1. As a control, mtDNA in BrdU-containing DNA was also amplified, and the results were presented as a percentage of mtDNA. For Cdk1 and Cdk2 bindings to origins, FM3A cells were cultured at 33 °C, and ChIP analysis was performed with α-Cdk1 and α-Cdk2 antibodies as described (14). The results were presented as a percentage of input.

ACKNOWLEDGMENTS. We thank Dr. C. Namikawa-Yamada, Mr. K. Murata, and Miss H. Kojima for technical assistance. This work was supported in part by the Ministry of Education, Science, Sports, and Culture of Japan through a Grant-in-Aid of Scientific Research (to M.N.).

1. Machida YJ, Hamlin JL, Dutta A (2005) Right place, right time, and only once: Replication. *Cell* 123:13–24.
2. Jackson DA (1995) Nuclear organization: Uniting replication foci, chromatin domains, and chromosome structure. *BioEssays* 17:587–591.
3. Woodward AM, *et al.* (2006) Excess Mcm2–7 license dormant origins of replication that can be used under conditions of replicative stress. *J Cell Biol* 173:673–683.
4. Shechter D, Gautier J (2005) ATM and ATR check in on origins: A dynamic model for origin selection and activation. *Cell Cycle* 4:235–238.
5. Shechter D, Costanzo V, Gautier J (2004) ATR and ATM regulate the timing of DNA replication origin firing. *Nat Cell Biol* 6:648–655.
6. Maya-Mendoza A, Petermann E, Gillespie DA, Caldecott KW, Jackson DA (2007) Chk1 regulates the density of active replication origins during the vertebrate S phase. *EMBO J* 26:2719–2731.
7. Niida H, *et al.* (2005) Depletion of Chk1 leads to premature activation of Cdc2-cyclin B and mitotic catastrophe. *J Biol Chem* 280:39246–39252.
8. Donaldson AD, *et al.* (1998) CLB5-dependent activation of late replication origins in *S. cerevisiae*. *Mol Cell* 2:173–182.
9. Heichinger C, Penkett CJ, Bähler J, Nurse P (2006) Genomewide characterization of fission yeast DNA replication origins. *EMBO J* 25:5171–5179.
10. Dai J, Chuang RY, Kelly TJ (2005) DNA replication origins in the *Schizosaccharomyces pombe* genome. *Proc Natl Acad Sci USA* 102:337–342.
11. Patel PK, Arcangioli B, Baker SP, Bensimon A, Rhind N (2006) DNA replication origins fire stochastically in fission yeast. *Mol Biol Cell* 17:308–316.
12. Jeon Y, *et al.* (2005) Temporal profile of replication of human chromosomes. *Proc Natl Acad Sci USA* 102:6419–6424.
13. Sadoni N, Cardoso MC, Stelzer EH, Leonhardt H, Zink D (2004) Stable chromosomal units determine the spatial and temporal organization of DNA replication. *J Cell Sci* 117:5353–5365.
14. Shimada M, *et al.* (2008) Chk1 is a histone H3 threonine 11 kinase that regulates DNA damage-induced transcriptional repression. *Cell* 132:221–232.
15. O'Keefe RT, Henderson SC, Spector DL (1992) Dynamic organization of DNA replication in mammalian cell nuclei: Spatially and temporally defined replication of chromosome-specific α-satellite DNA sequences. *J Cell Biol* 116:1095–1110.
16. Hiratani I, Leskovar A, Gilbert DM (2004) Differentiation-induced replication-timing changes are restricted to AT-rich/long interspersed nuclear element (LINE)-rich isochores. *Proc Natl Acad Sci USA* 101:16861–16866.
17. Aladjem MI, *et al.* (2002) Replication initiation patterns in the β-globin loci of totipotent and differentiated murine cells: Evidence for multiple initiation regions. *Mol Cell Biol* 22:442–452.
18. Jiang K, *et al.* (2003) Regulation of Chk1 includes chromatin association and 14–3-3 binding following phosphorylation on Ser-345. *J Biol Chem* 278:25207–25217.
19. Niida H, Katsuno Y, Banerjee B, Hande MP, Nakanishi M (2007) Specific role of Chk1 phosphorylations in cell survival and checkpoint activation. *Mol Cell Biol* 27:2572–2581.
20. Bartek J, Lukas J (2003) Chk1 and Chk2 kinases in checkpoint control and cancer. *Cancer Cell* 3:421–429.
21. Merrick KA, *et al.* (2008) Distinct activation pathways confer cyclin-binding specificity on cdk1 and cdk2 in human cells. *Mol Cell* 32:662–672.
22. Th'ng JP, *et al.* (1990) The FT210 cell line is a mouse G_2 phase mutant with a temperature-sensitive CDC2 gene product. *Cell* 63:313–324.
23. Romanowski P, *et al.* (2000) Interaction of *Xenopus* Cdc2 × cyclin A1 with the origin recognition complex. *J Biol Chem* 275:4239–4243.
24. Wuarin J, Buck V, Nurse P, Millar JB (2002) Stable association of mitotic cyclin B/Cdc2 to replication origins prevents endoreduplication. *Cell* 111:419–431.
25. Ge XQ, Jackson DA, Blow JJ (2007) Dormant origins licensed by excess Mcm2–7 are required for human cells to survive replicative stress. *Genes Dev* 21:3331–3341.
26. Hochegger H, *et al.* (2007) An essential role for Cdk1 in S phase control is revealed via chemical genetics in vertebrate cells. *J Cell Biol* 178:257–268.
27. Krasinska L, *et al.* (2008) Cdk1 and Cdk2 activity levels determine the efficiency of replication origin firing in *Xenopus*. *EMBO J* 27:758–769.
28. Porter AC (2008) Preventing DNA overreplication: A Cdk perspective. *Cell Div* 3:3.
29. Fujita M, *et al.* (1998) Cell cycle- and chromatin binding state-dependent phosphorylation of human MCM heterohexameric complexes: A role for cdc2 kinase. *J Biol Chem* 273:17095–17101.
30. Michalet X, *et al.* (1997) Dynamic molecular combing: Stretching the whole human genome for high-resolution studies. *Science* 277:1518–1523.
31. Sugimura K, Takebayashi S, Taguchi H, Takeda S, Okumura K (2008) PARP-1 ensures regulation of replication fork progression by homologous recombination on damaged DNA. *J Cell Biol* 183:1203–1212.

Efficient Generation of Functional Hepatocytes From Human Embryonic Stem Cells and Induced Pluripotent Stem Cells by HNF4α Transduction

Kazuo Takayama[1,2], Mitsuru Inamura[1,2], Kenji Kawabata[2,3], Kazufumi Katayama[1], Maiko Higuchi[2], Katsuhisa Tashiro[2], Aki Nonaka[2], Fuminori Sakurai[1], Takao Hayakawa[4,5], Miho Kusuda Furue[6,7] and Hiroyuki Mizuguchi[1,2,8]

[1]Laboratory of Biochemistry and Molecular Biology, Graduate School of Pharmaceutical Sciences, Osaka University, Osaka, Japan; [2]Laboratory of Stem Cell Regulation, National Institute of Biomedical Innovation, Osaka, Japan; [3]Laboratory of Biomedical Innovation, Graduate School of Pharmaceutical Sciences, Osaka University, Osaka, Japan; [4]Pharmaceutics and Medical Devices Agency, Tokyo, Japan; [5]Pharmaceutical Research and Technology Institute, Kinki University, Osaka, Japan; [6]JCRB Cell Bank, Division of Bioresources, National Institute of Biomedical Innovation, Osaka, Japan; [7]Laboratory of Cell Processing, Institute for Frontier Medical Sciences, Kyoto University, Kyoto, Japan; [8]The Center for Advanced Medical Engineering and Informatics, Osaka University, Osaka, Japan

Hepatocyte-like cells from human embryonic stem cells (ESCs) and induced pluripotent stem cells (iPSCs) are expected to be a useful source of cells drug discovery. Although we recently reported that hepatic commitment is promoted by transduction of SOX17 and HEX into human ESC- and iPSC-derived cells, these hepatocyte-like cells were not sufficiently mature for drug screening. To promote hepatic maturation, we utilized transduction of the hepatocyte nuclear factor 4α (HNF4α) gene, which is known as a master regulator of liver-specific gene expression. Adenovirus vector-mediated overexpression of HNF4α in hepatoblasts induced by SOX17 and HEX transduction led to upregulation of epithelial and mature hepatic markers such as cytochrome P450 (CYP) enzymes, and promoted hepatic maturation by activating the mesenchymal-to-epithelial transition (MET). Thus HNF4α might play an important role in the hepatic differentiation from human ESC-derived hepatoblasts by activating the MET. Furthermore, the hepatocyte like-cells could catalyze the toxication of several compounds. Our method would be a valuable tool for the efficient generation of functional hepatocytes derived from human ESCs and iPSCs, and the hepatocyte-like cells could be used for predicting drug toxicity.

Received 19 July 2011; accepted 28 September 2011; published online 8 November 2011. doi:10.1038/mt.2011.234

INTRODUCTION

Human embryonic stem cells (ESCs) and induced pluripotent stem cells (iPSCs) are able to replicate indefinitely and differentiate into most of the body's cell types.[1,2] They could provide an unlimited source of cells for various applications. Hepatocyte-like cells, which are differentiated from human ESCs and iPSCs, would be useful for basic research, regenerative medicine, and drug discovery.[3] In particular, it is expected that hepatocyte-like cells will be utilized as a tool for cytotoxicity screening in the early phase of pharmaceutical development. To catalyze the toxication of several compounds, hepatocyte-like cells need to be mature enough to exhibit hepatic functions, including high activity levels of the cytochrome P450 (CYP) enzymes. Because the present technology for the generation of hepatocyte-like cells from human ESCs and iPSCs, which is expected to be utilized for drug discovery, is not refined enough for this application, it is necessary to improve the efficiency of hepatic differentiation. Although conventional methods such as growth factor-mediated hepatic differentiation are useful to recapitulate liver development, they lead to only a heterogeneous hepatocyte population.[4–6] Recently, we showed that transcription factors are transiently transduced to promote hepatic differentiation in addition to the conventional differentiation method which uses only growth factors.[7] Ectopic expression of Sry-related HMG box 17 (SOX17) or hematopoietically expressed homeobox (HEX) by adenovirus (Ad) vectors in human ESC-derived mesendoderm or definitive endoderm (DE) cells markedly enhances the endoderm differentiation or hepatic commitment, respectively.[7,8] However, further hepatic maturation is required for drug screening.

The transcription factor hepatocyte nuclear factor 4α (HNF4α) is initially expressed in the developing hepatic diverticulum on E8.75,[9,10] and its expression is elevated as the liver develops. A previous loss-of-function study showed that HNF4α plays a critical role in liver development; conditional deletion of *HNF4α* in fetal hepatocytes results in the faint expression of many mature hepatic enzymes and the impairment of normal liver morphology.[11] The genome-scale chromatin immunoprecipitation assay showed that HNF4α binds to the promoters of nearly half of the genes expressed in the mouse liver,[12] including cell adhesion and junctional proteins,[13] which are important in

Correspondence: *Hiroyuki Mizuguchi, Laboratory of Biochemistry and Molecular Biology, Graduate School of Pharmaceutical Sciences, Osaka University, 1-6 Yamadaoka, Suita, Osaka 565-0871, Japan. E-mail: mizuguch@phs.osaka-u.ac.jp*

the hepatocyte epithelial structure.[14] In addition, HNF4α plays a critical role in hepatic differentiation and in a wide variety of liver functions, including lipid and glucose metabolism.[15,16] Although HNF4α could promote transdifferentiation into hepatic lineage from hematopoietic cells,[17] the function of HNF4α in hepatic differentiation from human ESCs and iPSCs remains unknown. A previous study showed that hepatic differentiation from mouse hepatic progenitor cells is promoted by HNF4α, although many of the hepatic markers that they examined were target genes of HNF4α.[18] They transplanted the HNF4α-overexpressed mouse hepatic progenitor cells to promote hepatic differentiation, but they did not examine the markers that relate to hepatic maturation such as CYP enzymes, conjugating enzymes, and hepatic transporters.

In this study, we examined the role of HNF4α in hepatic differentiation from human ESCs and iPSCs. The human ESC- and iPSC-derived hepatoblasts, which were efficiently generated by sequential transduction of SOX17 and HEX, were transduced with HNF4α-expressing Ad vector (Ad-HNF4α), and then the expression of hepatic markers of the hepatocyte-like cells were assessed. In addition, we examined whether or not the hepatocyte-like cells, which were generated by sequential transduction of SOX17, HEX, and HNF4α, were able to predict the toxicity of several compounds.

RESULTS

Stage-specific HNF4α transduction in hepatoblasts selectively promotes hepatic differentiation

The transcription factor HNF4α plays an important role in both liver generation[11] and hepatic differentiation from human ESCs and iPSCs (**Supplementary Figure S1**). We expected that hepatic differentiation could be accelerated by HNF4α transduction. To examine the effect of forced expression of HNF4α in the hepatic differentiation from human ESC- and iPSC-derived cells, we used a fiber-modified Ad vector.[19] Initially, we optimized the time period for Ad-HNF4α transduction. Human ESC (H9)-derived DE cells (day 6) (**Supplementary Figures S2** and **S3a**), hepatoblasts (day 9) (**Supplementary Figures S2** and **S3b**), or a heterogeneous population consisting of hepatoblasts, hepatocytes, and cholangiocytes (day 12) (**Supplementary Figures S2** and **S3c**) were transduced with Ad-HNF4α and then the Ad-HNF4α-transduced cells were cultured until day 20 of differentiation (**Figure 1**). We ascertained the expression of exogenous *HNF4α* in human ESC-derived hepatoblasts (day 9) transduced with Ad-HNF4α (**Supplementary Figure S4**). The transduction of Ad-HNF4α into human ESC-derived hepatoblasts (day 9) led to the highest expression levels of the hepatocyte markers *albumin* (*ALB*)[20] and *α-1-antitrypsin* (**Figure 1a**). In contrast, the expression levels of the cholangiocyte markers *cytokeratin 7* (*CK7*)[21] and *SOX9*[22] were

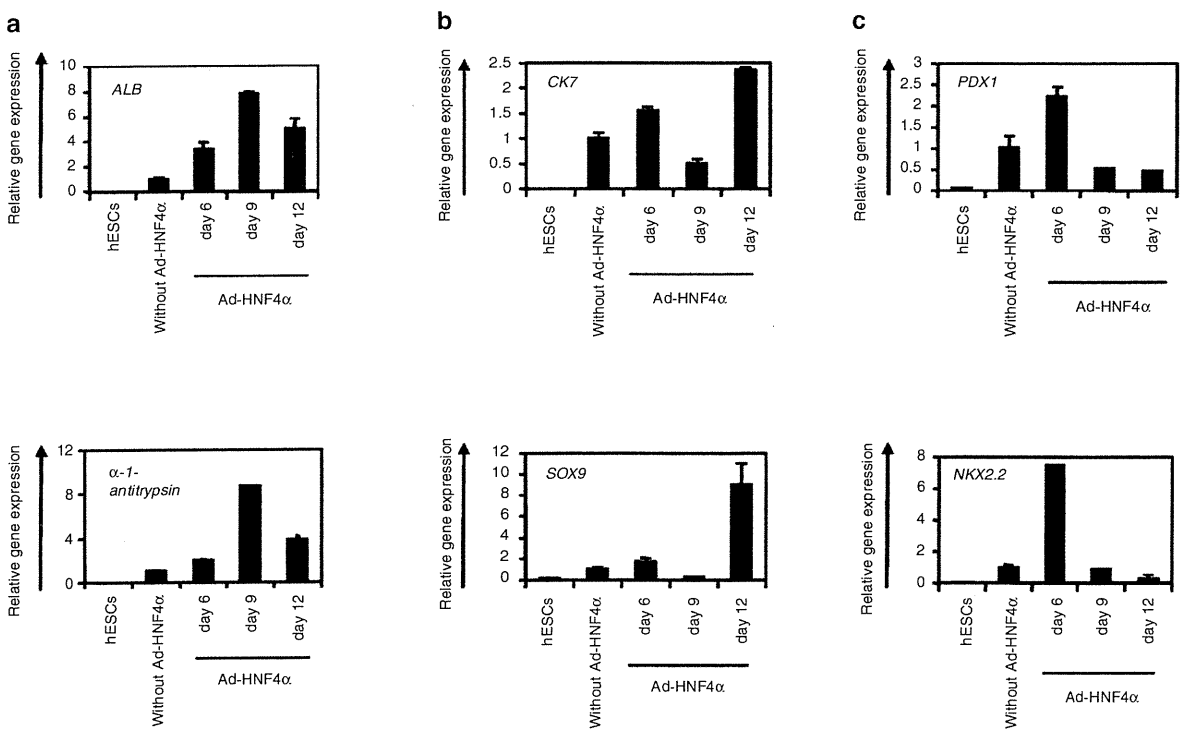

Figure 1 Transduction of HNF4α into hepatoblasts promotes hepatic differentiation. (**a–c**) The human ESC (H9)-derived cells, which were cultured for 6, 9, or 12 days according to the protocol described in **Figure 2a**, were transduced with 3,000 vector particles (VP)/cell of Ad-HNF4α for 1.5 hours and cultured until day 20. The gene expression levels of (**a**) hepatocyte markers (*ALB* and *α-1-antitrypsin*), (**b**) cholangiocyte markers (*CK7* and *SOX9*), and (**c**) pancreas markers (*PDX1* and *NKX2.2*) were examined by real-time RT-PCR on day 0 (human ESCs (hESCs)) or day 20 of differentiation. The horizontal axis represents the days when the cells were transduced with Ad-HNF4α. On the y-axis, the level of the cells without Ad-HNF4α transduction on day 20 was taken as 1.0. All data are represented as means ± SD (n = 3). ESC, embryonic stem cell; HNF4α, hepatocyte nuclear factor 4α; RT-PCR, reverse transcription-PCR.

downregulated in the cells transduced on day 9 as compared with nontransduced cells (**Figure 1b**). This might be because hepatic differentiation was selectively promoted and biliary differentiation was repressed by the transduction of HNF4α in hepatoblasts. The expression levels of the pancreas markers *PDX1*[23] and *NKX2.2*[24] did not make any change in the cells transduced on day 9 as compared with nontransduced cells (**Figure 1c**). Interestingly, the expression levels of the pancreas markers were upregulated, when Ad-HNF4α transduction was performed into DE cells (day 6) (**Figure 1c**). These results suggest that HNF4α might promote not only hepatic differentiation but also pancreatic differentiation, although the optimal stage of HNF4 transduction for the differentiation of each cell is different. We have confirmed that there was no difference between nontransduced cells and Ad-LacZ-transduced cells in the gene expression levels of all the markers investigated in **Figure 1a–c** (data not shown). We also confirmed that Ad vector-mediated gene expression in the human ESC-derived hepatoblasts (day 9) continued until day 14 and almost disappeared on day 18 (**Supplementary Figure S5**). These results indicated that the stage-specific HNF4α overexpression in human ESC-derived hepatoblasts (day 9) was essential for promoting efficient hepatic differentiation.

Transduction of HNF4α into human ESC- and iPSC-derived hepatoblasts efficiently promotes hepatic maturation

From the results of **Figure 1**, we decided to transduce hepatoblasts (day 9) with Ad-HNF4α. To determine whether hepatic maturation is promoted by Ad-HNF4α transduction, Ad-HNF4α-transduced cells were cultured until day 20 of differentiation according to the schematic protocol described in **Figure 2a**. After the hepatic maturation, the morphology of human ESCs was gradually changed into that of hepatocytes: polygonal with distinct round nuclei (day 20) (**Figure 2b**). Interestingly, a portion of the hepatocyte-like cells, which were ALB[20]-, CK18[21]-, CYP2D6-, and CYP3A4[25]-positive cells, had double nuclei, which was also observed in primary human hepatocytes (**Figure 2b,c**, and **Supplementary Figure S6**). We also examined the hepatic gene expression levels on day 20 of differentiation (**Figure 3a,b**). The gene expression analysis of *CYP1A2*, *CYP2C9*, *CYP2C19*, *CYP2D6*, *CYP3A4*, and *CYP7A1*[25] showed higher expression levels in all of Ad-SOX17-, Ad-HEX-, and Ad-HNF4α-transduced cells (three factors-transduced cells) as compared with those in both Ad-SOX17- and Ad-HEX-transduced cells (two factors-transduced cells) on day 20 (**Figure 3a**). The gene expression level of NADPH-CYP reductase

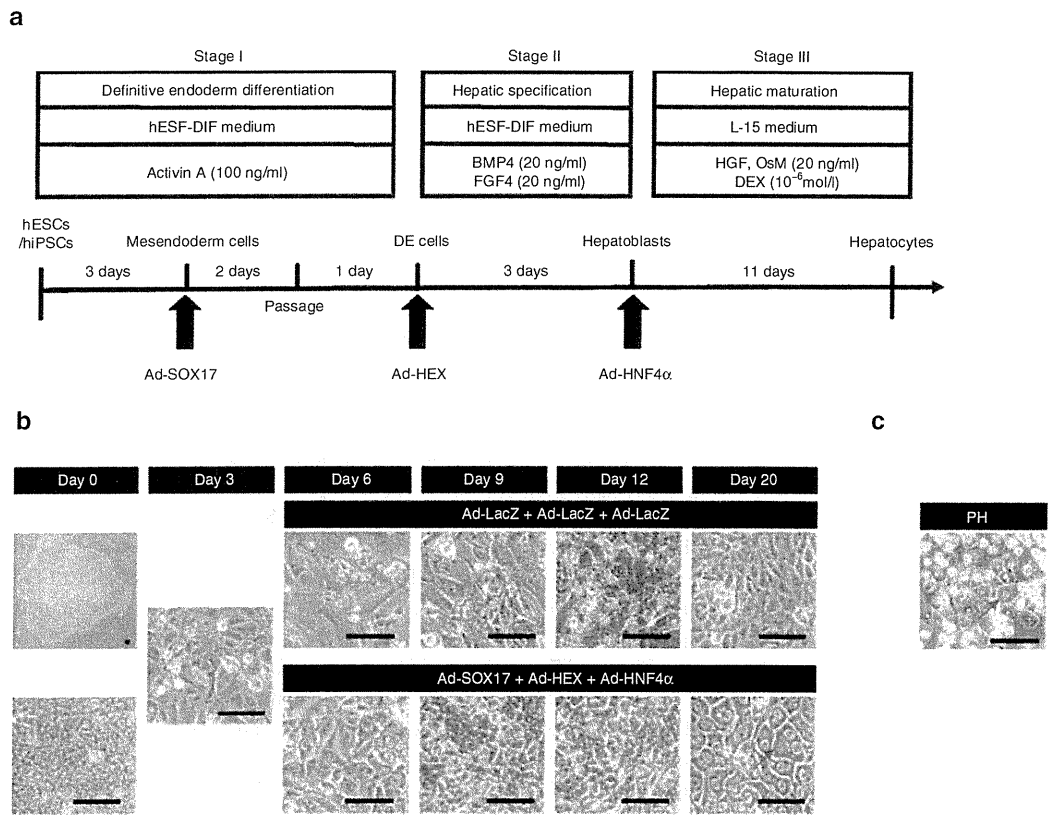

Figure 2 Hepatic differentiation of human ESCs and iPSCs transduced with three factors. (**a**) The procedure for differentiation of human ESCs and iPSCs into hepatocytes via DE cells and hepatoblasts is presented schematically. The hESF-DIF medium was supplemented with 10 μg/ml human recombinant insulin, 5 μg/ml human apotransferrin, 10 μmol/l 2-mercaptoethanol, 10 μmol/l ethanolamine, 10 μmol/l sodium selenite, and 0.5 mg/ml fatty-acid-free BSA. The L15 medium was supplemented with 8.3% tryptose phosphate broth, 8.3% FBS, 10 μmol/l hydrocortisone 21-hemisuccinate, 1 μmol/l insulin, and 25 mmol/l $NaHCO_3$. (**b**) Sequential morphological changes (day 0–20) of human ESCs (H9) differentiated into hepatocytes via DE cells and hepatoblasts are shown. Red arrow shows the cells that have double nuclei. (**c**) The morphology of primary human hepatocytes is shown. Bar represents 50 μm. BSA, bovine serum albumin; DE, definitive endoderm; ESC, embryonic stem cell; iPSC, induced pluripotent stem cell.

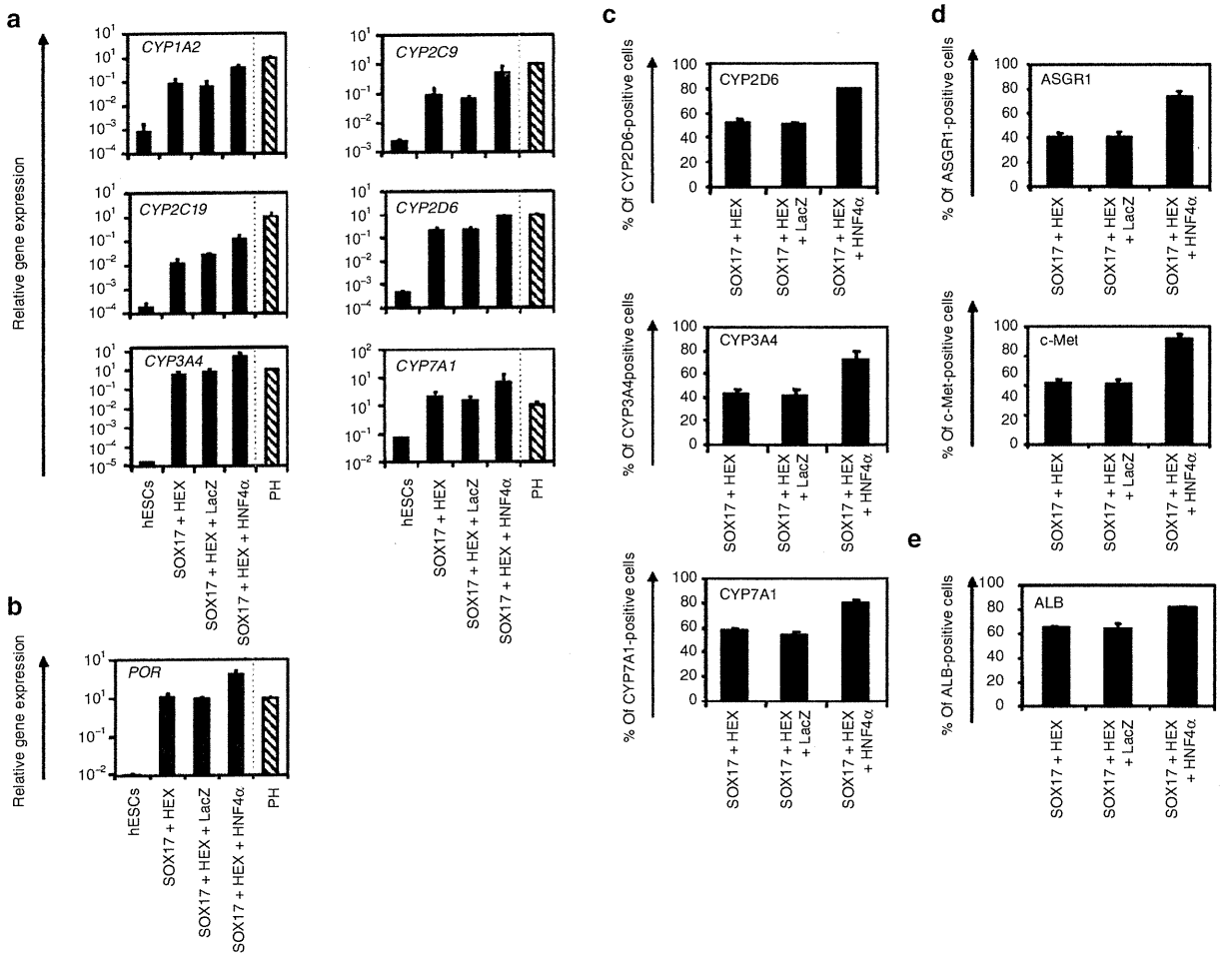

Figure 3 Transduction of HNF4α promotes hepatic maturation from human ESCs and iPSCs. (**a**,**b**) The human ESCs were differentiated into hepatocytes according to the protocol described in **Figure 2a**. On day 20 of differentiation, the gene expression levels of (**a**) CYP enzymes (*CYP1A2*, *CYP2C9*, *CYP2C19*, *CYP2D6*, *CYP3A4*, and *CYP7A1*) and (**b**) *POR* were examined by real-time RT-PCR in undifferentiated human ESCs (hESCs), the hepatocyte-like cells, and primary human hepatocytes (PH, hatched bar). On the y-axis, the expression level of primary human hepatocytes, which were cultured for 48 hours after the cells were plated, was taken as 1.0. (**c**–**e**) The hepatocyte-like cells (day 20) were subjected to immunostaining with (**c**) anti-drug-metabolizing enzymes (CYP2D6, CYP3A4, and CYP7A1), (**d**) anti-hepatic surface protein (ASGR1 and c-Met), and (**e**) anti-ALB antibodies, and then the percentage of antigen-positive cells was examined by flow cytometry on day 20 of differentiation. All data are represented as means ± SD (n = 3). ESC, embryonic stem cell; HNF4α, hepatocyte nuclear factor 4α; iPSC, induced pluripotent stem cell.

(POR)[26], which is required for the normal function of CYPs, was also higher in the three factors-transduced cells (**Figure 3b**). The gene expression analysis of ALB, α-1-antitrypsin (α-1-AT), transthyretin, hepatic conjugating enzymes, hepatic transporters, and hepatic transcription factors also showed higher expression levels in the three factors-transduced cells (**Supplementary Figures S7** and **S8**). Moreover, the gene expression levels of these hepatic markers of three factor-transduced cells were similar to those of primary human hepatocytes, although the levels depended on the type of gene (**Figure 3a,b**, and **Supplementary Figures S7** and **S8**). To confirm that similar results could be obtained with human iPSCs, we used three human iPS cell lines (201B7, Dotcom, and Tic). The gene expression of hepatic markers in human ESC- and iPSC-derived hepatocytes were analyzed by real-time reverse transcription-PCR on day 20 of differentiation. Three human iPS cell lines as well as human ESCs also effectively differentiated into hepatocytes in response to transduction of the three factors (**Supplementary Figure S9**). Interestingly, we observed differences in the hepatic maturation efficiency among the three human iPS cell lines. That is, two of the human iPS cell lines (Tic and Dotcom) were more committed to the hepatic lineage than another human iPS cell line (201B7). Because almost homogeneous hepatocyte-like cells would be more useful in basic research, regenerative medicine, and drug discovery, we also examined whether our novel methods for hepatic maturation could generate a homogeneous hepatocyte population by flow cytometry analysis (**Figure 3c–e**). The percentages of CYP2D6-, CYP3A4-, and CYP7A1-positive cells were ~80% in the three factors-transduced cells, while they were ~50% in the two factors-transduced cells (**Figure 3c**). The percentages of hepatic surface antigen (asialoglycoprotein receptor 1 (ASGR1] and met proto-oncogene (c-Met))-positive cells (**Figure 3d**) and ALB-positive cells (**Figure 3e**) were also ~80% in the three factors-transduced cells. These results indicated that a nearly homogeneous population was obtained by our differentiation protocol

using the transduction of three functional genes (SOX17, HEX, and HNF4α).

The three factors-transduced cells have characteristics of functional hepatocytes

The hepatic functions of the hepatocyte-like cells, such as the uptake of low-density lipoprotein (LDL) and CYP enzymes activity, of the hepatocyte-like cells were examined on day 20 of differentiation. Approximately 87% of the three factors-transduced cells uptook LDL in the medium, whereas only 44% of the two factors-transduced cells did so (**Figure 4a**). The activities of CYP enzymes of the hepatocyte-like cells were measured according to the metabolism of the CYP3A4, CYP2C9, or CYP1A2 substrates (**Figure 4b**). The metabolites were detected in the three factors-transduced cells and their activities were higher than those of the two factors-transduced cells (dimethyl sulfoxide (DMSO) column). We further tested the induction of CYP3A4, CYP2C9, and CYP1A2 by chemical stimulation, since CYP3A4, CYP2C9, and CYP1A2 are the important prevalent CYP isozymes in the liver and are involved in the metabolism of a significant proportion of the currently available commercial drugs (rifampicin or omeprazole column). It is well known that CYP3A4 and CYP2C9 can be induced by rifampicin, whereas CYP1A2 can be induced by omeprazole. The hepatocyte-like cells were treated with either of these. Although undifferentiated human ESCs responsed to neither rifampicin nor omeprazole (data not shown), the hepatocyte-like cells produced more metabolites in response to chemical stimulation as well as primary hepatocytes (**Figure 4b**). The activity levels of the hepatocyte-like cells as compared with those of primary human hepatocytes depended on the types of CYP; the CYP3A4 activity of the hepatocyte-like cells was similar to that of primary human hepatocytes, whereas the CYP2C9 and CYP1A2 activities of the hepatocyte-like cells were slightly lower than those of primary human hepatocytes (**Figure 3a**). These results indicated that high levels of functional CYP enzymes were detectable in the hepatocyte-like cells.

The metabolism of diverse compounds involving uptake, conjugation, and the subsequent release of the compounds is an important function of hepatocytes. Uptake and release of Indocyanine green (ICG) can often be used to identify hepatocytes in ESC differentiation models.[27] To investigate this function in our hepatocyte-like cells, we compared this ability of the three factors-transduced cells with that of the two factors-transduced cells on day 20 of differentiation (**Figure 4c**). The three factors-transduced cells had more ability to uptake ICG and to excrete ICG by culturing without ICG for 6 hours. We also examined whether the hepatocyte-like cells could store glycogen, a characteristic of functional hepatocytes (**Figure 4d**). On day 20 of differentiation, the three factors-transduced cells and the two factors-transduced cells were stained for cytoplasmic glycogen using the Periodic Acid-Schiff staining procedure. The three factors-transduced cells exhibited more abundant storage of glycogen than the two-factors-transduced cells. These results showed that abundant hepatic functions, such as uptake and excretion of ICG and storage of glycogen, were obtained by the transduction of three factors.

Many adverse drug reactions are caused by the CYP-dependent activation of drugs into reactive metabolites.[28] In order to examine metabolism-mediated toxicity and to improve the safety of drug candidates, primary human hepatocytes are widely used.[28] Because primary human hepatocytes have quite different characteristics among distinct lots and because it is difficult to purchase large amounts of primary human hepatocytes that have the same characteristics, hepatocyte-like cells are expected to be used for this purpose. To examine whether our hepatocyte-like cells could be used to predict metabolism-mediated toxicity, the hepatocyte-like cells were incubated with four substrates (troglitazone, acetaminophen, cyclophosphamide, and carbamazepine), which are known to generate toxic metabolites by CYP enzymes, and then the cell viability was measured (**Figure 4e**). The cell viability of the two factors plus Ad-LacZ-tansduced cells were higher than that of the three factors-transduced cells at each different concentration of four test compounds. These results indicated that the three factors-transduced cells could more efficiently metabolize the test compounds and thereby induce higher toxicity than either the two factors-transduced cells or undifferentiated human ESCs. The cell viability of the three factors-transduced cells was slightly higher than that of primary human hepatocytes.

HNF4α promotes hepatic maturation by activating mesenchymal-to-epithelial transition

HNF4α is known as a dominant regulator of the epithelial phenotype because its ectopic expression in fibroblasts (such as NIH 3T3 cells) induces mesenchymal-to-epithelial transition (MET)[11], although it is not known whether HNF4α can promote MET in hepatic differentiation. Therefore, we examined whether HNF4α transduction promotes hepatic maturation from hepatoblasts by activating MET. To clarify whether MET is activated by HNF4α transduction, the human ESC-derived hepatoblasts (day 9) were transduced with Ad-LacZ or Ad-HNF4α, and the resulting phenotype was analyzed on day 12 of differentiation (**Figure 5**). This time, we confirmed that HNF4α transduction decreased the population of N-cadherin (hepatoblast marker)-positive cells,[29] whereas it increased that of ALB (hepatocyte marker)-positive cells (**Figure 5a**). The number of CK7 (cholangiocyte marker)-positive population did not change (**Figure 5a**). To investigate whether these results were attributable to MET, the alteration of the expression of several mesenchymal and epithelial markers was examined (**Figure 5b**). The human ESC-derived hepatoblasts (day 9) were almost homogeneously N-cadherin[30] (mesenchymal marker)-positive and E-cadherin[11] (epithelial marker)-negative, demonstrating that human ESC-derived hepatoblasts have mesenchymal characteristics (**Figure 5a,b**). After HNF4α transduction, the number of E-cadherin-positive cells was increased and reached ~90% on day 20, whereas that of N-cadherin-positive cells was decreased and was less than 5% on day 20 (**Supplementary Figure S10**). These results indicated that MET was promoted by HNF4α transduction in hepatic differentiation from hepatoblasts. Interestingly, the number of growing cells was decreased by HNF4α transduction (**Figure 5c**), and the cell growth was delayed by HNF4α transduction (**Supplementary Figure S11**). This decrease in the number of growing cells might have been because the differentiation was promoted by HNF4α transduction. We also confirmed that MET was promoted by HNF4α transduction in the gene expression levels (**Figure 5d**).

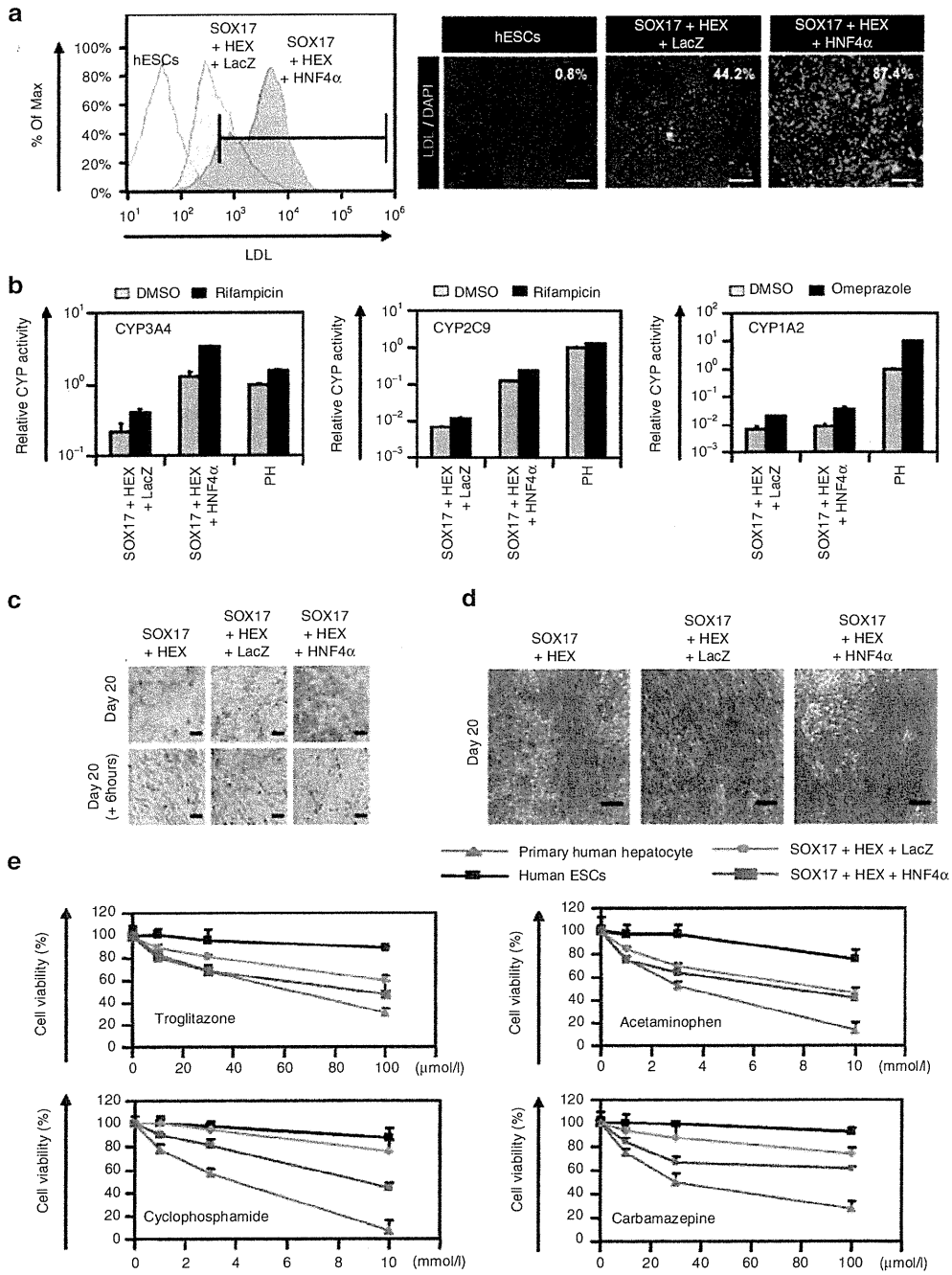

Figure 4 Transduction of the three factors enhances hepatic functions. The human ESCs were differentiated into hepatoblasts and transduced with 3,000 VP/cell of Ad-LacZ or Ad-HNF4α for 1.5 hours and cultured until day 20 of differentiation according to the protocol described in **Figure 2a**. The hepatic functions of the two factors plus Ad-LacZ-transduced cells (SOX17+HEX+LacZ) and the three factors-transduced cells (SOX17+HEX+HNF4α) were compared. (**a**) Undifferentiated human ESCs (hESCs) and the hepatocyte-like cells (day 20) were cultured with medium containing Alexa-Flour 488-labeled LDL (green) for 1 hour, and immunohistochemistry and flow cytometry analysis were performed. The percentage of LDL-positive cells was measured by flow cytometry. Nuclei were counterstained with DAPI (blue). The bar represents 100 μm. (**b**) Induction of CYP3A4 (left), CYP2C9 (middle), or CYP1A2 (right) by DMSO (gray bar), rifampicin (black bar), or omeprazole (black bar) in the hepatocyte-like cells (day 20) and primary human hepatocytes (PH), which were cultured for 48 hours after the cells were plated. On the y-axis, the activity of primary human hepatocytes that have been cultured with medium containing DMSO was taken as 1.0. (**c**) The hepatocyte-like cells (day 20) (upper column) were examined for their ability to take up Indocyanin Green (ICG) and release it 6 hours thereafter (lower column). (**d**) Glycogen storage of the hepatocyte-like cells (day 20) was assessed by Periodic Acid-Schiff (PAS) staining. PAS staining was performed on day 20 of differentiation. Glycogen storage is indicated by pink or dark red-purple cytoplasms. The bar represents 100 μm. (**e**) The cell viability of undifferentiated human ESCs (black), two factors plus Ad-LacZ-tansduced cells (green), the three factors-transduced cells (blue), and primary human hepatocytes (red) was assessed by Alamar Blue assay after 48 hours exposure to different concentrations of four test compounds (troglitazone, acetaminophen, cyclophosphamide, and carbamazepine). The cell viability is expressed as a percentage of cells treated with solvent only treat: 0.1% DMSO except for carbamazepine: 0.5% DMSO. All data are represented as means ± SD ($n = 3$). ESC, embryonic stem cell; DMSO, dimethyl sulfoxide; LDL, low-density lipoprotein.

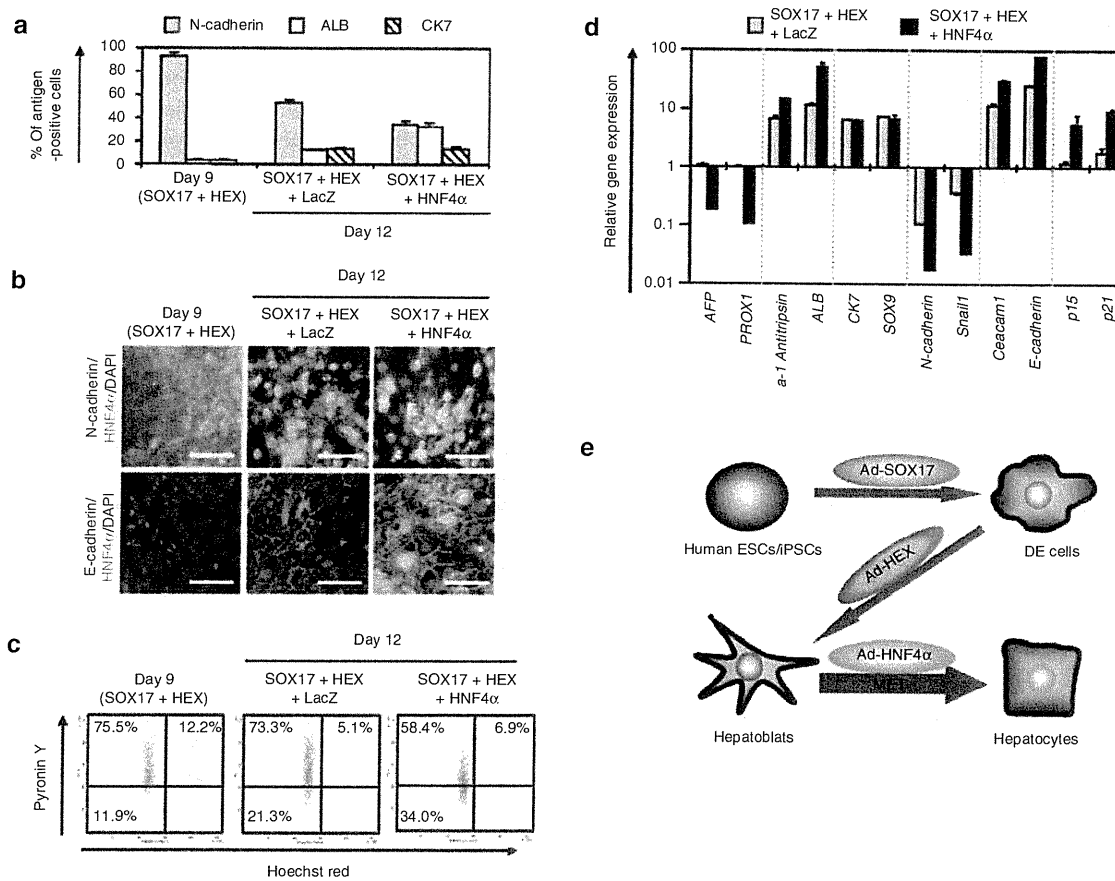

Figure 5 HNF4α promotes hepatic differentiation by activating MET. Human ESCs were differentiated into hepatoblasts according to the protocol described in **Figure 2a**, and then transduced with 3,000 VP/cell of Ad-LacZ or Ad-HNF4α for 1.5 hours, and finally cultured until day 12 of differentiation. (**a**) The hepatoblasts, two factors plus Ad-LacZ-transduced cells (SOX17+HEX+LacZ) (day 12), and the three factors-transduced cells (SOX17+HEX+HNF4α) (day 12) were subjected to immunostaining with anti-N-cadherin, ALB, or CK7 antibodies. The percentage of antigen-positive cells was measured by flow cytometry. (**b**) The cells were subjected to immunostaining with anti-N-cadherin (green), E-cadherin (green), or HNF4α (red) antibodies on day 9 or day 12 of differentiation. Nuclei were counterstained with DAPI (blue). The bar represents 50 μm. Similar results were obtained in two independent experiments. (**c**) The cell cycle was examined on day 9 or day 12 of differentiation. The cells were stained with Pyronin Y (y-axis) and Hoechst 33342 (x-axis) and then analyzed by flow cytometry. The growth fraction of cells is the population of actively dividing cells (G1/S/G2/M). (**d**) The expression levels of *AFP*, *PROX1*, *α-1-antitrypsin*, *ALB*, *CK7*, *SOX9*, *N-cadherin*, *Snail1*, *Ceacam1*, *E-cadherin*, *p15*, and *p21* were examined by real-time RT-PCR on day 9 or day 12 of differentiation. The expression level of hepatoblasts (day 9) was taken as 1.0. All data are represented as means ± SD ($n = 3$). (**e**) The model of efficient hepatic differentiation from human ESCs and iPSCs in this study is summarized. The human ESCs and iPSCs differentiate into hepatocytes via definitive endoderm and hepatoblasts. At each stage, the differentiation is promoted by stage-specific transduction of appropriate functional genes. In the last stage of hepatic differentiation, HNF4α transduction provokes hepatic maturation by activating MET. ESC, embryonic stem cell; HNF4α, hepatocyte nuclear factor 4α; iPSC, induced pluripotent stem cell; MET, mesenchymal-to-epithelial transition; RT-PCR, reverse transcription-PCR; VP, vector particle.

The gene expression levels of hepatocyte markers (*α-1-antitrypsin* and *ALB*)[20] and epithelial markers (*Ceacam1* and *E-cadherin*) were upregulated by HNF4α transduction. On the other hand, the gene expression levels of hepatoblast markers (*AFP* and *PROX1*)[31], mesenchymal markers (*N-cadherin* and *Snail*)[32], and cyclin dependent kinase inhibitor (*p15* and *p21*)[33] were downregulated by HNF4α transduction. HNF4α transduction did not change the expression levels of cholangiocyte markers (*CK7* and *SOX9*). We conclude that HNF4α promotes hepatic maturation by activating MET.

DISCUSSION

This study has two main purposes: the generation of functional hepatocytes from human ESCs and iPSCs for application to drug toxicity screening in the early phase of pharmaceutical development and; elucidation of the HNF4α function in hepatic maturation from human ESCs. We initially confirmed the importance of transcription factor HNF4α in hepatic differentiation from human ESCs by using a published data set of gene array analysis (**Supplementary Figure S1**).[34] We speculated that HNF4α transduction could enhance hepatic differentiation from human ESCs and iPSCs.

To generate functional hepatocytes from human ESCs and iPSCs and to elucidate the function of HNF4α in hepatic differentiation from human ESCs, we examined the stage-specific roles of HNF4α. We found that hepatoblast (day 9) stage-specific HNF4α transduction promoted hepatic differentiation (**Figure 1**). Because endogenous HNF4α is initially expressed in the hepatoblast,[9,10] our system might adequately reflect early embryogenesis. However, HNF4α transduction at an inappropriate stage (day 6 or day 12) promoted

bidirectional differentiation; heterogeneous populations, which contain the hepatocytes and pancreas cells or hepatocytes and cholangiocytes, were obtained, respectively (**Figure 1**), consistent with a previous report that HNF4α plays an important role not only in the liver but also in the pancreas.[12] Therefore, we concluded that HNF4α plays a significant stage-specific role in the differentiation of human ESC- and iPSC-derived hepatoblasts to hepatocytes (**Figure 5e**).

We found that the expression levels of the hepatic functional genes were upregulated by HNF4α transduction (**Figure 3a,b**, and **Supplementary Figures S7** and **S8**). Although the c/EBPα and GATA4 expression levels of the three factors-transduced cells were higher than those of primary human hepatocytes, the FOXA1, FOXA2, FOXA3, and HNF1α, which are known to be important for hepatic direct reprogramming and hepatic differentiation,[35,36] expression levels of three factors-transduced cells were slightly lower than those of primary human hepatocytes (**Supplementary Figure S8**). Therefore, additional transduction of FOXA1, FOXA2, FOXA3, and HNF1α might promote further hepatic maturation. Some previous hepatic differentiation protocols that utilized growth factors without gene transfer led to the appearance only of heterogeneous hepatocyte populations.[4–6] The HNF4α transduction led not only to the upregulation of expression levels of several hepatic markers but also to an almost homogeneous hepatocyte population; the differentiation efficacy based on CYPs, ASGR1, or ALB expression was ~80% (**Figure 3c–e**). The efficient hepatic maturation in this study might be attributable to the activation of many hepatocyte-associated genes by the transduction of HNF4α, which binds to the promoters of nearly half of the genes expressed in the liver.[12] In the later stage of hepatic maturation, hepatocyte-associated genes would be strongly upregulated by endogenous transcription factors but not exogenous HNF4α because transgene expression by Ad vectors was almost disappeared on day 18 (**Supplementary Figure S5**). Another reason for the efficient hepatic maturation would be that sequential transduction of SOX17, HEX, and HNF4α could mimic hepatic differentiation in early embryogenesis.

Next, we examined whether or not the hepatocyte-like cells had hepatic functions. The activity of many kinds of CYPs was upregulated by HNF4α transduction (**Figure 4b**). Ad-HNF4α-transduced cells exhibit many characteristics of hepatocytes: uptake of LDL, uptake and excretion of ICG, and storage of glycogen (**Figure 4a,c,d**). Many conventional tests of hepatic characteristics have shown that the hepatocyte-like cells have mature hepatocyte functions. Furthermore, the hepatocyte-like cells can catalyze the toxication of several compounds (**Figure 4e**). Although the activities to catalyze the toxication of test compounds in primary human hepatocytes are slightly higher than those in the hepatocyte-like cells, the handling of primary human hepatocytes is difficult for a number of reasons: since their source is limited, large-scale primary human hepatocytes are difficult to prepare as a homogeneous population. Therefore, the hepatocyte-like cells derived from human ESCs and iPSCs would be a valuable tool for predicting drug toxicity. To utilize the hepatocyte-like cells in a drug toxicity study, further investigation of the drug metabolism capacity and CYP induction potency will be needed.

We also investigated the mechanisms underlying efficient hepatic maturation by HNF4α transduction. Although the number of cholangiocyte populations did not change by HNF4α transduction, we found that the number of hepatoblast populations decreased and that of hepatocyte populations increased, indicating that HNF4α promotes selective hepatic differentiation from hepatoblasts (**Figure 5a**). As previously reported, HNF4α regulates the expression of a broad range of genes that code for cell adhesion molecules,[13] extracellular matrix components, and cytoskeletal proteins, which determine the main morphological characteristics of epithelial cells.[14,35,37] In this study, we elucidated that MET was promoted by HNF4α transduction (**Figure 5b,d**). Thus, we conclude that HNF4α overexpression in hepatoblasts promotes hepatic differentiation by activating MET (**Figure 5e**).

Using human iPSCs as well as human ESCs, we confirmed that the stage-specific overexpression of HNF4α could promote hepatic maturation (**Supplementary Figure S9**). Interestingly, the differentiation efficacies differed among human iPS cell lines: two of the human iPS cell lines (Dotcom and Tic) were more committed to the hepatic lineage than another human iPS cell line (201B7) (**Supplementary Figure S7**). Therefore, it would be necessary to select a human iPS cell line that is suitable for hepatic maturation in the case of medical applications, such as drug screening and liver transplantation. The difference of hepatic differentiation efficacy among the three iPSC lines might be due to the difference of epigenetic memory of original cells or the difference of the inserted position of the foreign genes for the reprogramming.

To control hepatic differentiation mimicking embryogenesis, we employed Ad vectors, which are one of the most efficient transient gene delivery vehicles and have been widely used in both experimental studies and clinical trials.[38] We used a fiber-modified Ad vector containing the EF-1α promoter and a stretch of lysine residue (KKKKKKK, K7) peptides in the C-terminal region of the fiber knob.[19] The K7 peptide targets heparan sulfates on the cellular surface, and the fiber-modified Ad vector containing the K7 peptides was shown to be efficient for transduction into many kinds of cells including human ESCs and human ESC-derived cells.[7–8,19] Thus, Ad vector-mediated transient gene transfer should be a powerful tool for regulating cellular differentiation.

In summary, the findings described here demonstrate that transcription factor HNF4α plays a crucial role in the hepatic differentiation from human ESC-derived hepatoblasts by activating MET (**Figure 5e**). In the present study, both human ESCs and iPSCs (three lines) were used and all cell lines showed efficient hepatic maturation, indicating that our protocol would be a universal tool for cell line-independent differentiation into functional hepatocytes. Moreover, the hepatocyte-like cells can catalyze the toxication of several compounds as primary human hepatocytes. Therefore, our technology, by sequential transduction of SOX17, HEX, and HNF4α, would be a valuable tool for the efficient generation of functional hepatocytes derived from human ESCs and iPSCs, and the hepatocyte-like cells could be used for the prediction of drug toxicity.

MATERIALS AND METHODS

Human ESC and iPSC culture. A human ES cell line, H9 (WiCell Research Institute, Madison, HI), was maintained on a feeder layer of mitomycin C-treated mouse embryonic fibroblasts (Millipore, Billerica, MA) with Repro Stem (Repro CELL, Tokyo, Japan) supplemented with 5 ng/ml fibroblast

growth factor 2 (FGF2) (Sigma, St Louis, MO). Human ESCs were dissociated with 0.1 mg/ml dispase (Roche Diagnostics, Indianapolis, IN) into small clumps and then were subcultured every 4 or 5 days. H9 was used following the Guidelines for Derivation and Utilization of Human Embryonic Stem Cells of the Ministry of Education, Culture, Sports, Science and Technology of Japan. Two human iPS cell lines generated from the human embryonic lung fibroblast cell line MCR5 were provided from the JCRB Cell Bank (Tic, JCRB Number: JCRB1331; and Dotcom, JCRB Number: JCRB1327).[39,40] These human iPS cell lines were maintained on a feeder layer of mitomycin C-treated mouse embryonic fibroblasts with iPSellon (Cardio, Kobe, Japan) supplemented with 10 ng/ml FGF2. Another human iPS cell line, 201B7, generated from human dermal fibroblasts was kindly provided by Dr S. Yamanaka (Kyoto University).[2] The human iPS cell line 201B7 was maintained on a feeder layer of mitomycin C-treated mouse embryonic fibroblasts with Repro Stem (Repro CELL) supplemented with 5 ng/ml FGF2 (Sigma). Human iPSCs were dissociated with 0.1 mg/ml dispase (Roche Diagnostics) into small clumps and were then subcultured every 5 or 6 days.

In vitro *differentiation.* Before the initiation of cellular differentiation, the medium of human ESCs and iPSCs was exchanged for a defined serum-free medium, hESF9, and cultured as we previously reported.[41] hESF9 consists of hESF-GRO medium (Cell Science & Technology Institute, Sendai, Japan) supplemented with 10 μg/ml human recombinant insulin, 5 μg/ml human apotransferrin, 10 μmol/l 2-mercaptoethanol, 10 μmol/l ethanolamine, 10 μmol/l sodium selenite, oleic acid conjugated with fatty-acid-free bovine albumin (BSA), 10 ng/ml FGF2, and 100 ng/ml heparin (all from Sigma).

The differentiation protocol for the induction of DE cells, hepatoblasts, and hepatocytes was based on our previous report with some modifications.[7] Briefly, in mesendoderm differentiation, human ESCs and iPSCs were dissociated into single cells and cultured for 3 days on Matrigel (Becton, Dickinson and Company, Tokyo, Japan) in hESF-DIF medium (Cell Science & Technology Institute) supplemented with 10 μg/ml human recombinant insulin, 5 μg/ml human apotransferrin, 10 μmol/l 2-mercaptoethanol, 10 μmol/l ethanolamine, 10 μmol/l sodium selenite, 0.5 mg/ml BSA, and 100 ng/ml Activin A (R&D Systems, Minneapolis, MN). To generate mesendoderm cells and DE cells, human ESC-derived cells were transduced with 3,000 vector particles (VP)/cell of Ad-SOX17 for 1.5 hours on day 3 and cultured until day 6 on Matrigel (BD) in hESF-DIF medium (Cell Science & Technology Institute) supplemented with 10 μg/ml human recombinant insulin, 5 μg/ml human apotransferrin, 10 μmol/l 2-mercaptoethanol, 10 μmol/l ethanolamine, 10 μmol/l sodium selenite, 0.5 mg/ml BSA, and 100 ng/ml Activin A (R&D Systems). For induction of hepatoblasts, the DE cells were transduced with 3,000 VP/cell of Ad-HEX for 1.5 hours on day 6 and cultured for 3 days on a Matrigel (BD) in hESF-DIF (Cell Science & Technology Institute) medium supplemented with the 10 μg/ml human recombinant insulin, 5 μg/ml human apotransferrin, 10 μmol/l 2-mercaptoethanol, 10 μmol/l ethanolamine, 10 μmol/l sodium selenite, 0.5 mg/ml BSA, 20 ng/ml bone morphogenetic protein 4 (R&D Systems), and 20 ng/ml FGF4 (R&D Systems). In hepatic differentiation, hepatoblasts were transduced with 3,000 VP/cell of Ad-LacZ or Ad-HNF4α for 1.5 hr on day 9 and were cultured for 11 days on Matrigel (BD) in L15 medium (Invitrogen, Carlsbad, CA) supplemented with 8.3% tryptose phosphate broth (BD), 8.3% fetal bovine serum (Vita, Chiba, Japan), 10 μmol/l hydrocortisone 21-hemisuccinate (Sigma), 1 μmol/l insulin, 25 mmol/l $NaHCO_3$ (Wako, Osaka, Japan), 20 ng/ml hepatocyte growth factor (R&D Systems), 20 ng/ml Oncostatin M (R&D Systems), and 10^{-6} mol/l Dexamethasone (Sigma).

Ad vectors. Ad vectors were constructed by an improved *in vitro* ligation method.[42,43] The human HNF4α gene (accession number NM_000457) was amplified by PCR using primers designed to incorporate the 5′ Not I and 3′ Xba I restriction enzyme sites: Fwd 5′-ggcctctagatggaggcagggagaatg-3′ and Rev 5′-ccccgcggccgcagcggcttgctagataac-3′. The human HNF4α gene was inserted into pBSKII (Invitrogen), resulting in pBSKII-HNF4α, and then the human HNF4α gene was inserted into pHMEF5,[44] which contains the human elongation factor-1α (EF-1α) promoter, resulting in pHMEF-HNF4α. The pHMEF-HNF4α was digested with I-CeuI/PI-SceI and ligated into I-Ceu I/PI-SceI-digested pAdHM41-K7,[19] resulting in pAd-HNF4α. The human EF-1α promoter-driven LacZ-, SOX17-, or HEX-expressing Ad vectors, Ad-LacZ, Ad-SOX17, or Ad-HEX, were constructed previously.[7,8,45] Ad-LacZ, Ad-SOX17, Ad-HEX, and Ad-HNF4α, each of which contains a stretch of lysine residue (K7) peptides in the C-terminal region of the fiber knob for more efficient transduction of human ESCs, iPSCs, and DE cells, were generated and purified as described previously.[7] The VP titer was determined by using a spectrophotometric method.[46]

LacZ assay. Human ESC- and iPSC-derived cells were transduced with Ad-LacZ at 3,000 VP/cell for 1.5 hours. After culturing for the indicated number of days, 5-bromo-4-chloro-3-indolyl β-D-galactopyranoside (X-Gal) staining was performed as described previously.[44]

Flow cytometry. Single-cell suspensions of human ESCs, iPSCs, and their derivatives were fixed with methanol at 4 °C for 20 minutes and then incubated with the primary antibody, followed by the secondary antibody. Flow cytometry analysis was performed using a FACS LSR Fortessa flow cytometer (BD).

RNA isolation and reverse transcription-PCR. Total RNA was isolated from human ESCs, iPSCs, and their derivatives using ISOGENE (Nippon Gene) according to the manufacturer's instructions. Primary human hepatocytes were purchased from CellzDirect, Durham, NC. complementary DNA was synthesized using 500 ng of total RNA with a Superscript VILO cDNA synthesis kit (Invitrogen). Real-time reverse transcription-PCR was performed with Taqman gene expression assays (Applied Biosystems, Foster City, CA) or SYBR Premix Ex Taq (TaKaRa) using an ABI PRISM 7000 Sequence Detector (Applied Biosystems). Relative quantification was performed against a standard curve and the values were normalized against the input determined for the housekeeping gene, glyceraldehyde 3-phosphate dehydrogenase. The primer sequences used in this study are described in **Supplementary Table S1**.

Immunohistochemistry. The cells were fixed with methanol or 4% paraformaldehyde (Wako). After blocking with phosphate-buffered saline containing 2% BSA (Sigma) and 0.2% Triton X-100 (Sigma), the cells were incubated with primary antibody at 4 °C for 16 hours, followed by incubation with a secondary antibody that was labeled with Alexa Fluor 488 (Invitrogen) or Alexa Fluor 594 (Invitrogen) at room temperature for 1 hour. All the antibodies are listed in **Supplementary Table S2**.

Assay for CYP activity. To measure cytochrome P450 3A4, 2C9, and 1A2 activity, we performed Lytic assays by using a P450-GloTM CYP3A4 Assay Kit (Promega, Madison, WI). For the CYP3A4 and 2C9 activity assay, undifferentiated human ESCs, the hepatocyte-like cells, and primary human hepatocytes were treated with rifampicin (Sigma), which is the substrate for CYP3A4 and CYP2C9, at a final concentration of 25 μmol/l or DMSO (0.1%) for 48 hours. For the CYP1A2 activity assay, undifferentiated human ESCs, the hepatocyte-like cells, and primary human hepatocytes were treated with omeprazole (Sigma), which is the substrate for CYP1A2, at a final concentration of 10 μM or DMSO (0.1%) for 48 hours. We measured the fluorescence activity with a luminometer (Lumat LB 9507; Berthold, Oak Ridge, TN) according to the manufacturer's instructions.

Pyronin Y/Hoechst Staining. Human ESC-derived cells were stained with Hoechst33342 (Sigma) and Pyronin Y (PY) (Sigma) in Dulbecco's modified Eagle medium (Wako) supplemented with 0.2 mmol/l HEPES and 5% FCS (Invitrogen). Samples were then placed on ice for 15 minutes, and 7-AAD was added to a final concentration of 0.5 mg/ml for exclusion of dead cells. Fluorescence-activated cell-sorting analysis of these cells was

performed on a FACS LSR Fortessa flow cytometer (Becton Dickinson) equipped with a UV-laser.

Cellular uptake and excretion of ICG. ICG (Sigma) was dissolved in DMSO at 100 mg/ml, then added to a culture medium of the hepatocyte-like cells to a final concentration of 1 mg/ml on day 20 of differentiation. After incubation at 37 °C for 60 minutes, the medium with ICG was discarded and the cells were washed with phosphate-buffered saline. The cellular uptake of ICG was then examined by microscopy. Phosphate-buffered saline was then replaced by the culture medium and the cells were incubated at 37 °C for 6 hours. The excretion of ICG was examined by microscopy.

Periodic Acid-Schiff assay for glycogen. The hepatocyte-like cells were fixed with 4% paraformaldehyde and stained using a Periodic Acid-Schiff staining system (Sigma) on day 20 of differentiation according to the manufacturer's instructions.

Cell viability tests. Cell viability was assessed by Alamar Blue assay kit (Invitrogen). After treatment with test compounds[47–50] (troglitazone, acetaminophen, cyclophosphamide, and carbamazepine) (all from Wako) for 2 days, the culture medium was replaced with 0.5 mg/ml solution of Alamar Blue in culturing medium and cells were incubated for 3 hours at 37 °C. The supernatants of the cells were measured at a wavelength of 570 nm with background subtraction at 600 nm in a plate reader. Control refers to incubations in the absence of test compounds and was considered as 100% viability value.

Uptake of LDL. The hepatocyte-like cells were cultured with medium containing Alexa-488-labeled LDL (Invitrogen) for 1 hour, and then the cells that could uptake LDL were assessed by immunohistochemistry and flow cytometry.

Primary human hepatocytes. Cryopreserved human hepatocytes were purchased from CellzDirect (lot Hu8072). The vials of hepatocytes were rapidly thawed in a shaking water bath at 37 °C; the contents of the vial were emptied into prewarmed Cryopreserved Hepatocyte Recovery Medium (CellzDirect) and the suspension was centrifuged at 100*g* for 10 minutes at room temperature. The hepatocytes were seeded at 1.25×10^5 cells/cm^2 in hepatocyte culture medium (Lonza, Walkersville, MD) containing 10% FCS (GIBCO-BRL) onto type I collagen-coated 12-well plates. The medium was replaced with hepatocyte culture medium containing 10% FCS (GIBCO-BRL) 6 hours after seeding. The hepatocytes, which were cultured 48 hours after plating the cells, were used in the experiments.

SUPPLEMENTARY MATERIAL

Figure S1. Genome-wide screening of transcription factors involved in hepatic differentiation emphasizes the importance of the transcription factor HNF4α.
Figure S2. Summary of specific markers for DE cells, hepatoblasts, hepatocytes, cholangiocytes, and pancreas cells.
Figure S3. The formation of DE cells, hepatoblasts, hepatocytes, and cholangiocytes from human ESCs.
Figure S4. Overexpression of HNF4α mRNA in hepatoblasts by Ad-HNF4α transduction.
Figure S5. Time course of LacZ expression in hepatoblasts transduced with Ad-LacZ.
Figure S6. The morphology of the hepatocyte-like cells.
Figure S7. Upregulation of the expression levels of conjugating enzymes and hepatic transporters by HNF4α transduction.
Figure S8. Upregulation of the expression levels of hepatic transcription factors by HNF4α transduction.
Figure S9. Generation of hepatocytes from various human ES or iPS cell lines.
Figure S10. Promotion of MET by HNF4α transduction.
Figure S11. Arrest of cell growth by HNF4α transduction.
Table S1. List of Taqman probes and primers used in this study.
Table S2. List of antibodies used in this study.

ACKNOWLEDGMENTS

We thank Hiroko Matsumura and Misae Nishijima for their excellent technical support. H.M., M.K.F., and T.H. were supported by grants from the Ministry of Health, Labor, and Welfare of Japan. H.M. was also supported by Japan Research foundation For Clinical Phamacology, The Nakatomi Foundation, and The Uehara Memorial Foundation. K.K. (K. Kawabata) was supported by grants from the Ministry of Education, Sports, Science and Technology of Japan (20200076) and the Ministry of Health, Labor, and Welfare of Japan. K.K. (K. Katayama) and F.S. was supported by Program for Promotion of Fundamental Studies in Health Sciences of the National Institute of Biomedical Innovation (NIBIO).

REFERENCES

1. Thomson, JA, Itskovitz-Eldor, J, Shapiro, SS, Waknitz, MA, Swiergiel, JJ, Marshall, VS *et al.* (1998). Embryonic stem cell lines derived from human blastocysts. *Science* **282**: 1145–1147.
2. Takahashi, K, Tanabe, K, Ohnuki, M, Narita, M, Ichisaka, T, Tomoda, K *et al.* (2007). Induction of pluripotent stem cells from adult human fibroblasts by defined factors. *Cell* **131**: 861–872.
3. Murry, CE and Keller, G (2008). Differentiation of embryonic stem cells to clinically relevant populations: lessons from embryonic development. *Cell* **132**: 661–680.
4. Basma, H, Soto-Gutiérrez, A, Yannam, GR, Liu, L, Ito, R, Yamamoto, T *et al.* (2009). Differentiation and transplantation of human embryonic stem cell-derived hepatocytes. *Gastroenterology* **136**: 990–999.
5. Touboul, T, Hannan, NR, Corbineau, S, Martinez, A, Martinet, C, Branchereau, S *et al.* (2010). Generation of functional hepatocytes from human embryonic stem cells under chemically defined conditions that recapitulate liver development. *Hepatology* **51**: 1754–1765.
6. Duan, Y, Ma, X, Ma, X, Zou, W, Wang, C, Bahbahan, IS *et al.* (2010). Differentiation and characterization of metabolically functioning hepatocytes from human embryonic stem cells. *Stem Cells* **28**: 674–686.
7. Inamura, M, Kawabata, K, Takayama, K, Tashiro, K, Sakurai, F, Katayama, K *et al.* (2011). Efficient generation of hepatoblasts from human ES cells and iPS cells by transient overexpression of homeobox gene HEX. *Mol Ther* **19**: 400–407.
8. Takayama, K, Inamura, M, Kawabata, K, Tashiro, K, Katayama, K, Sakurai, F *et al.* (2011). Efficient and directive generation of two distinct endoderm lineages from human ESCs and iPSCs by differentiation stage-specific SOX17 transduction. *PLoS ONE* **6**: e21780.
9. Duncan, SA, Manova, K, Chen, WS, Hoodless, P, Weinstein, DC, Bachvarova, RF *et al.* (1994). Expression of transcription factor HNF-4 in the extraembryonic endoderm, gut, and nephrogenic tissue of the developing mouse embryo: HNF-4 is a marker for primary endoderm in the implanting blastocyst. *Proc Natl Acad Sci USA* **91**: 7598–7602.
10. Taraviras, S, Monaghan, AP, Schütz, G and Kelsey, G (1994). Characterization of the mouse HNF-4 gene and its expression during mouse embryogenesis. *Mech Dev* **48**: 67–79.
11. Parviz, F, Matullo, C, Garrison, WD, Savatski, L, Adamson, JW, Ning, G *et al.* (2003). Hepatocyte nuclear factor 4alpha controls the development of a hepatic epithelium and liver morphogenesis. *Nat Genet* **34**: 292–296.
12. Odom, DT, Zizlsperger, N, Gordon, DB, Bell, GW, Rinaldi, NJ, Murray, HL *et al.* (2004). Control of pancreas and liver gene expression by HNF transcription factors. *Science* **303**: 1378–1381.
13. Battle, MA, Konopka, G, Parviz, F, Gaggl, AL, Yang, C, Sladek, FM *et al.* (2006). Hepatocyte nuclear factor 4alpha orchestrates expression of cell adhesion proteins during the epithelial transformation of the developing liver. *Proc Natl Acad Sci USA* **103**: 8419–8424.
14. Konopka, G, Tekiela, J, Iverson, M, Wells, C and Duncan, SA (2007). Junctional adhesion molecule-A is critical for the formation of pseudocanaliculi and modulates E-cadherin expression in hepatic cells. *J Biol Chem* **282**: 28137–28148.
15. Li, J, Ning, G and Duncan, SA (2000). Mammalian hepatocyte differentiation requires the transcription factor HNF-4alpha. *Genes Dev* **14**: 464–474.
16. Hayhurst, GP, Lee, YH, Lambert, G, Ward, JM and Gonzalez, FJ (2001). Hepatocyte nuclear factor 4alpha (nuclear receptor 2A1) is essential for maintenance of hepatic gene expression and lipid homeostasis. *Mol Cell Biol* **21**: 1393–1403.
17. Khurana, S, Jaiswal, AK and Mukhopadhyay, A (2010). Hepatocyte nuclear factor-4alpha induces transdifferentiation of hematopoietic cells into hepatocytes. *J Biol Chem* **285**: 4725–4731.
18. Suetsugu, A, Nagaki, M, Aoki, H, Motohashi, T, Kunisada, T and Moriwaki, H (2008). Differentiation of mouse hepatic progenitor cells induced by hepatocyte nuclear factor-4 and cell transplantation in mice with liver fibrosis. *Transplantation* **86**: 1178–1186.
19. Koizumi, N, Mizuguchi, H, Utoguchi, N, Watanabe, Y and Hayakawa, T (2003). Generation of fiber-modified adenovirus vectors containing heterologous peptides in both the HI loop and C terminus of the fiber knob. *J Gene Med* **5**: 267–276.
20. Shiojiri, N (1984). The origin of intrahepatic bile duct cells in the mouse. *J Embryol Exp Morphol* **79**: 25–39.
21. Moll, R, Franke, WW, Schiller, DL, Geiger, B and Krepler, R (1982). The catalog of human cytokeratins: patterns of expression in normal epithelia, tumors and cultured cells. *Cell* **31**: 11–24.

22. Antoniou, A, Raynaud, P, Cordi, S, Zong, Y, Tronche, F, Stanger, BZ *et al.* (2009). Intrahepatic bile ducts develop according to a new mode of tubulogenesis regulated by the transcription factor SOX9. *Gastroenterology* **136**: 2325–2333.
23. Offield, MF, Jetton, TL, Labosky, PA, Ray, M, Stein, RW, Magnuson, MA *et al.* (1996). PDX-1 is required for pancreatic outgrowth and differentiation of the rostral duodenum. *Development* **122**: 983–995.
24. Sussel, L, Kalamaras, J, Hartigan-O'Connor, DJ, Meneses, JJ, Pedersen, RA, Rubenstein, JL *et al.* (1998). Mice lacking the homeodomain transcription factor Nkx2.2 have diabetes due to arrested differentiation of pancreatic beta cells. *Development* **125**: 2213–2221.
25. Ingelman-Sundberg, M, Oscarson, M and McLellan, RA (1999). Polymorphic human cytochrome P450 enzymes: an opportunity for individualized drug treatment. *Trends Pharmacol Sci* **20**: 342–349.
26. Henderson, CJ, Otto, DM, Carrie, D, Magnuson, MA, McLaren, AW, Rosewell, I *et al.* (2003). Inactivation of the hepatic cytochrome P450 system by conditional deletion of hepatic cytochrome P450 reductase. *J Biol Chem* **278**: 13480–13486.
27. Yamada, T, Yoshikawa, M, Kanda, S, Kato, Y, Nakajima, Y, Ishizaka, S *et al.* (2002). *In vitro* differentiation of embryonic stem cells into hepatocyte-like cells identified by cellular uptake of indocyanine green. *Stem Cells* **20**: 146–154.
28. Anzenbacher, P and Anzenbacherová, E (2001). Cytochromes P450 and metabolism of xenobiotics. *Cell Mol Life Sci* **58**: 737–747.
29. Zhao, D, Chen, S, Cai, J, Guo, Y, Song, Z, Che, J *et al.* (2009). Derivation and characterization of hepatic progenitor cells from human embryonic stem cells. *PLoS ONE* **4**: e6468.
30. Hatta, K, Takagi, S, Fujisawa, H and Takeichi, M (1987). Spatial and temporal expression pattern of N-cadherin cell adhesion molecules correlated with morphogenetic processes of chicken embryos. *Dev Biol* **120**: 215–227.
31. Shiojiri, N (1981). Enzymo- and immunocytochemical analyses of the differentiation of liver cells in the prenatal mouse. *J Embryol Exp Morphol* **62**: 139–152.
32. Lee, JM, Dedhar, S, Kalluri, R and Thompson, EW (2006). The epithelial-mesenchymal transition: new insights in signaling, development, and disease. *J Cell Biol* **172**: 973–981.
33. Macleod, KF, Sherry, N, Hannon, G, Beach, D, Tokino, T, Kinzler, K *et al.* (1995). p53-dependent and independent expression of p21 during cell growth, differentiation, and DNA damage. *Genes Dev* **9**: 935–944.
34. Si-Tayeb, K, Noto, FK, Nagaoka, M, Li, J, Battle, MA, Duris, C *et al.* (2010). Highly efficient generation of human hepatocyte-like cells from induced pluripotent stem cells. *Hepatology* **51**: 297–305.
35. Sekiya, S and Suzuki, A (2011). Direct conversion of mouse fibroblasts to hepatocyte-like cells by defined factors. *Nature* **475**: 390–393.
36. Huang, P, He, Z, Ji, S, Sun, H, Xiang, D, Liu, C *et al.* (2011). Induction of functional hepatocyte-like cells from mouse fibroblasts by defined factors. *Nature* **475**: 386–389.
37. Satohisa, S, Chiba, H, Osanai, M, Ohno, S, Kojima, T, Saito, T *et al.* (2005). Behavior of tight-junction, adherens-junction and cell polarity proteins during HNF-4alpha-induced epithelial polarization. *Exp Cell Res* **310**: 66–78.
38. Xu, ZL, Mizuguchi, H, Sakurai, F, Koizumi, N, Hosono, T, Kawabata, K *et al.* (2005). Approaches to improving the kinetics of adenovirus-delivered genes and gene products. *Adv Drug Deliv Rev* **57**: 781–802.
39. Nagata, S, Toyoda, M, Yamaguchi, S, Hirano, K, Makino, H, Nishino, K *et al.* (2009). Efficient reprogramming of human and mouse primary extra-embryonic cells to pluripotent stem cells. *Genes Cells* **14**: 1395–1404.
40. Makino, H, Toyoda, M, Matsumoto, K, Saito, H, Nishino, K, Fukawatase, Y *et al.* (2009). Mesenchymal to embryonic incomplete transition of human cells by chimeric OCT4/3 (POU5F1) with physiological co-activator EWS. *Exp Cell Res* **315**: 2727–2740.
41. Furue, MK, Na, J, Jackson, JP, Okamoto, T, Jones, M, Baker, D *et al.* (2008). Heparin promotes the growth of human embryonic stem cells in a defined serum-free medium. *Proc Natl Acad Sci USA* **105**: 13409–13414.
42. Mizuguchi, H and Kay, MA (1998). Efficient construction of a recombinant adenovirus vector by an improved *in vitro* ligation method. *Hum Gene Ther* **9**: 2577–2583.
43. Mizuguchi, H and Kay, MA (1999). A simple method for constructing E1- and E1/E4-deleted recombinant adenoviral vectors. *Hum Gene Ther* **10**: 2013–2017.
44. Kawabata, K, Sakurai, F, Yamaguchi, T, Hayakawa, T and Mizuguchi, H (2005). Efficient gene transfer into mouse embryonic stem cells with adenovirus vectors. *Mol Ther* **12**: 547–554.
45. Tashiro, K, Kawabata, K, Sakurai, H, Kurachi, S, Sakurai, F, Yamanishi, K *et al.* (2008). Efficient adenovirus vector-mediated PPAR gamma gene transfer into mouse embryoid bodies promotes adipocyte differentiation. *J Gene Med* **10**: 498–507.
46. Maizel, JV Jr, White, DO and Scharff, MD (1968). The polypeptides of adenovirus. I. Evidence for multiple protein components in the virion and a comparison of types 2, 7A, and 12. *Virology* **36**: 115–125.
47. Smith, MT (2003). Mechanisms of troglitazone hepatotoxicity. *Chem Res Toxicol* **16**: 679–687.
48. Dai, Y and Cederbaum, AI (1995). Cytotoxicity of acetaminophen in human cytochrome P4502E1-transfected HepG2 cells. *J Pharmacol Exp Ther* **273**: 1497–1505.
49. Chang, TK, Weber, GF, Crespi, CL and Waxman, DJ (1993). Differential activation of cyclophosphamide and ifosphamide by cytochromes P-450 2B and 3A in human liver microsomes. *Cancer Res* **53**: 5629–5637.
50. Miao, XS and Metcalfe, CD (2003). Determination of carbamazepine and its metabolites in aqueous samples using liquid chromatography-electrospray tandem mass spectrometry. *Anal Chem* **75**: 3731–3738.

Biochemical and Biophysical Research Communications 416 (2011) 119–124

Contents lists available at SciVerse ScienceDirect

Biochemical and Biophysical Research Communications

journal homepage: www.elsevier.com/locate/ybbrc

Use of human hepatocyte-like cells derived from induced pluripotent stem cells as a model for hepatocytes in hepatitis C virus infection

Takeshi Yoshida [a,1], Kazuo Takayama [b,1], Masuo Kondoh [a,*], Fuminori Sakurai [b], Hideki Tani [c], Naoya Sakamoto [d], Yoshiharu Matsuura [c], Hiroyuki Mizuguchi [b,*], Kiyohito Yagi [a]

[a] Laboratory of Bio-Functional Molecular Chemistry, Graduate School of Pharmaceutical Sciences, Osaka University, Osaka, Japan
[b] Laboratory of Biochemistry and Molecular Biology, Graduate School of Pharmaceutical Sciences, Osaka University, Osaka, Japan
[c] Department of Molecular Virology, Research Institute for Microbial Diseases, Osaka University, Osaka, Japan
[d] Department of Gastroenterology and Hepatology, Tokyo Medical and Dental University, Tokyo, Japan

ARTICLE INFO

Article history:
Received 31 October 2011
Available online 10 November 2011

Keywords:
Hepatitis C virus
Induced pluripotent stem cell
Hepatocyte
Infection
Replication
Experimental model

ABSTRACT

Host tropism of hepatitis C virus (HCV) is limited to human and chimpanzee. HCV infection has never been fully understood because there are few conventional models for HCV infection. Human induced pluripotent stem cell-derived hepatocyte-like (iPS-Hep) cells have been expected to use for drug discovery to predict therapeutic activities and side effects of compounds during the drug discovery process. However, the suitability of iPS-Hep cells as an experimental model for HCV research is not known. Here, we investigated the entry and genomic replication of HCV in iPS-Hep cells by using HCV pseudotype virus (HCVpv) and HCV subgenomic replicons, respectively. We showed that iPS-Hep cells, but not iPS cells, were susceptible to infection with HCVpv. The iPS-Hep cells expressed HCV receptors, including CD81, scavenger receptor class B type I (SR-BI), claudin-1, and occludin; in contrast, the iPS cells showed no expression of SR-BI or claudin-1. HCV RNA genome replication occurred in the iPS-Hep cells. Anti-CD81 antibody, an inhibitor of HCV entry, and interferon, an inhibitor of HCV genomic replication, dose-dependently attenuated HCVpv entry and HCV subgenomic replication in iPS-Hep cells, respectively. These findings suggest that iPS-Hep cells are an appropriate model for HCV infection.

1. Introduction

Hepatitis C virus (HCV), a hepatotropic member of the *Flaviviridae* family, is the leading cause of chronic hepatitis, cirrhosis and hepatocellular carcinoma. Approximately 130–200 million people are estimated to be infected with HCV worldwide. Each year, 3–4 million people are newly infected with HCV [1]. Thus, overcoming HCV is a critical issue for the World Health Organization.

HCV contains a positive strand ~9.6 kb RNA encoding a single polyprotein (~3000 aa), which is cleaved by host and viral proteases to form structural proteins (core, E1, E2, and p7) and nonstructural proteins (NS2, NS3, NS4A, NS4B, NS5A, and NS5B) [1]. These virus proteins might be potent targets for anti-HCV drugs. However, combination therapy with interferon and ribavirin, which often causes severe side-effects leading to treatment termination, has been the only therapeutic choice [2]. Very recently, new direct antiviral agents have been approved or are under clinical trials; these agents include NS3 protease inhibitors, NS5A inhibitors, and NS5B polymerase inhibitors [2–4]. However, the emergence of drug resistance is a serious problem associated with the use of direct antiviral agents [5].

Host targets are alternative targets for the development of anti-HCV drugs. A liver-specific microRNA (miRNA), miR-122, facilitates the replication of the HCV RNA genome in cultured liver cells [6]. Administration of a chemically modified oligonucleotide complementary to miR-122 results in long-lasting suppression of HCV with no appearance of resistant HCV in chimpanzees [7]. Epidermal

Abbreviations: HCV, hepatitis C virus; iPS-Hep cells, human induced pluripotent stem cells-derived hepatocyte-like cells; HCVpv, HCV pseudotype virus; SR-BI, scavenger receptor class B type I; miRNA, microRNA; EGF-R, epidermal growth factor receptor; EphA2, ephrin factor A2; iPS cells, human induced pluripotent stem cells; FCS, fetal calf serum; Ad, adenovirus; HNF-4α, hepatocyte nuclear factor-4α; RT, reverse transcription; PCR, polymerase chain reaction; GAPDH, glyceraldehyde 3-phosphate dehydrogenase; VSV, vesicular stomatitis virus; VSVpv, VSV pseudotype virus; tet, tetracycline; pol, polymerase; MOI, multiplicity of infection; Dox, doxycycline; IFN, interferon-α8; ES cells, embryonic stem cells.

* Corresponding authors. Address: Laboratory of Bio-Functional Molecular Chemistry, Graduate School of Pharmaceutical Sciences, Osaka University, Suita, Osaka 565-0871, Japan. Fax: +81 6 6879 8199 (M. Kondoh); Laboratory of Biochemistry and Molecular Biology, Graduate School of Pharmaceutical Sciences, Osaka University, Suita, Osaka 565-0871, Japan. Fax: +81 6 6879 8185 (H. Mizuguchi).

E-mail addresses: masuo@phs.osaka-u.ac.jp (M. Kondoh), mizuguch@phs.osaka-u.ac.jp (H. Mizuguchi).

[1] These authors contributed equally to this study.

0006-291X/$ - see front matter © 2011 Elsevier Inc. All rights reserved.
doi:10.1016/j.bbrc.2011.11.007

growth factor receptor (EGF-R) and ephrin factor A2 (EphA2) are host cofactors for HCV entry [8]. Inhibitors of EGF-R and EphA2 attenuated HCV entry, and prevented the appearance of viral escape variants [8]. These findings strongly indicate that identification of host factors associated with infection of human liver by HCV is a potent strategy for anti-HCV drug development. Because the host tropism of HCV is limited to human and chimpanzee [9], there is no convenient model for the evaluation of HCV infections. This has led to a delay in the development of anti-HCV agents targeting host factors.

Takahashi and Yamanaka developed human induced pluripotent stem (iPS) cells from human somatic cells [10]. The stem cells can be redifferentiated *in vitro*, leading to new models for drug discovery, including iPS-based models for drug discovery, toxicity assessment, and disease modeling [11,12].

Recently, several groups reported that iPS cells can be successfully differentiated into hepatocyte-like (iPS-Hep) cells that show many functions associated with mature hepatocytes [13–19]. However, whether iPS-Hep cells are suitable as a model for HCV infection has not been fully determined. Here, we investigated HCV entry and genomic replication in iPS-Hep cells by using HCV pseudotype virus (HCVpv) and HCV subgenomic replicons, respectively.

2. Materials and methods

2.1. Cell culture

Huh7 cells were cultured in Dulbecco's modified Eagle's medium supplemented with 10% fetal calf serum (FCS). An iPS cell-line (Dotcom) generated from the human embryonic lung fibroblast cell-line MCR5 was obtained from the Japanese Collection of Research Bioresources Cell Bank [20,21]. The iPS cells were maintained on a feeder layer of mitomycin C-treated mouse embryonic fibroblasts (Millipore, Billerica, MA) in iPSellon culture medium (Cardio, Hyogo, Japan) supplemented with 10 ng/ml fibroblast growth factor-2.

2.2. In vitro differentiation

Before the initiation of cellular differentiation, the medium of the iPS cells was replaced with a defined serum-free medium, hESF9, and the cells were cultured as previously reported [22]. The iPS cells were differentiated into iPS-Hep cells by using adenovirus (Ad) vectors expressing SOX17, the homeotic gene HEX or hepatocyte nuclear factor 4α (HNF-4α) in addition to the appropriate growth factors, cytokines, and supplements, as described previously [19].

2.3. Reverse transcription (RT)-polymerase chain reaction (PCR) analysis of HCV receptors

Total RNA samples were reverse-transcribed using the SuperScript VILO cDNA Synthesis Kit (Invitrogen, Carlsbad, CA), and the resultant cDNAs were PCR amplified by using Ex Taq DNA polymerase (TaKaRa Bio Inc., Shiga, Japan) and specific paired-primers for CD81 (5′-cgccaaggatgtgaagcagttc-3′ and 5′-tcccggagaagaggtcatcgat-3′), scavenger receptor class B type I (SR-BI; 5′-attccgatcagtgcaacatga-3′ and 5′-cagttttgcttcctgcagcacag-3′), claudin-1 (5′-tcagcactgccctgccccagt-3′ and 5′-tggtgttgggtaagaggttgt-3′), occludin (5′-tcagggaatatccacctatcacttcag-3′ and 5′-catcagcagcagccatgtactcttcac-3′), or glyceraldehyde 3-phosphate dehydrogenase (GAPDH) (5′-tcttcaccaccatggagaag-3′ and 5′-accacctggtgctcagtgta-3′). The expected sizes of the PCR products were 245 bp for CD81, 788 bp for SR-BI, 521 bp for claudin-1, 189 bp for occludin, and 544 bp for GAPDH. The PCR products were separated on 2% agarose gels and visualized by staining with ethidium bromide.

2.4. HCVpv infection

Pseudotype vesicular stomatitis virus (VSV) bearing HCV envelope glycoproteins (HCVpv) and VSV envelope glycoproteins (VSVpv) were prepared as described previously [23]. iPS, iPS-Hep and Huh7 cells were treated with HCVpv or mixtures of HCVpv or VSVpv and anti-CD81 monoclonal antibody (JS-81; BD Biosciences, Franklin Lakes, NJ) or control mouse IgG for 2 h. After an additional 24 h of culture, the luciferase activities were measured by using a commercially available kit (PicaGene, Toyo Ink, Tokyo, Japan).

2.5. Preparation of Ad vector expressing the HCV replicon

Ad vectors expressing a tetracycline (tet)-controllable and RNA polymerase (pol) I promoter-driven HCV subgenomic replicon containing renilla luciferase (AdP$_I$235-HCV), a replication-incompetent HCV subgenomic replicon containing renilla luciferase (AdP$_I$235-ΔGDD), tet-responsive trans-activator (Ad-tTA) or a tet-controllable RNA pol-I driven firefly luciferase (AdP$_I$235-fluc) were prepared by using an *in vitro* ligation method as described previously [24–26]. The biological activity (infectious unit) of the Ad vectors was measured by using an Adeno-X rapid titer kit (Clontech, Mountain View, CA).

2.6. HCV replication assay

iPS, iPS-Hep and Huh7 cells were infected with AdP$_I$235-HCV or AdP$_I$235-ΔGDD at multiplicity of infection (MOI; infectious unit per cell) of 3, and Ad-tTA at MOI of 15. After 24 h, the cells were treated with 10 μg/ml of doxycycline (Dox) for 48 h. Renilla luciferase activities in the lysates were then measured with the use of the Renilla Luciferase Assay System (Promega, Madison, WI). To normalize for the infectivity of Ad vector, iPS, iPS-Hep and Huh7 cells were co-infected with AdP$_I$235-fluc (3 MOI) and Ad-tTA (15 MOI). After a 72-h incubation, the firefly luciferase activities in the lysates were measured, and the renilla luciferase activities were normalized by dividing by the corresponding firefly luciferase activities.

2.7. Quantitative analysis of plus- and minus-strand HCV RNA

iPS, iPS-Hep and Huh7 cells were co-infected with AdP$_I$235-HCV or AdP$_I$235-ΔGDD (3 MOI), and Ad-tTA (15 MOI). After 24 h, the cells were treated with 10 μg/ml of Dox for 48 h. Total RNA was reverse-transcribed into cDNA by using the Thermoscript reverse transcriptase kit (Invitrogen) as described previously [27,28]. Real-time PCR was performed with SYBR Premix Ex Taq (TaKaRa Bio Inc.) by using Applied Biosystems StepOne Plus (Applied Biosystems, Foster City, CA). The transcription products of the HCV plus-strand RNA, minus-strand RNA, and GAPDH gene, were amplified by using specific primers for HCV plus-strand RNA (RC1 primer, 5′-gtctagccatggcgttagta-3′; and RC21 primer, 5′-ctcccggggcactcgcaagc-3′), HCV minus-strand RNA (tag primer, 5′-ggccgtcatggtggcgaataa-3′; and RC21 primer), and GAPDH (5′-ggtggtctcctctgacttcaaca-3′ and 5′-gtggtcgttgagggcaatg-3′), respectively. The copy numbers of the transcription products of the HCV plus- and minus-strand RNA were normalized with those of the GAPDH gene and infectivity of Ad vector as described in the Section 2.6.

2.8. Inhibition of HCV replication by interferon-α8

iPS-Hep and Huh7 cells were infected with AdP$_I$235-HCV (3 MOI) and Ad-tTA (15 MOI). After 24 h of infection, the cells were treated with 10 μg/ml of Dox and recombinant human interferon-α8 (IFN) at the indicated concentration. After an additional 48-h incubation, renilla luciferase activity in the lysates was measured with the use of the Renilla Luciferase Assay System. Cell

viability was measured with the use of a WST-8 kit (Nacalai Tesque, Kyoto, Japan).

3. Results

3.1. Infection of iPS-Hep cells with HCVpv

HCV entry requires sequential interaction between the envelope proteins and multiple cellular factors, including CD81, SR-BI, claudin-1, and occludin [29]. To investigate expression of these receptors in iPS-Hep cells, we performed RT-PCR analysis. iPS cells expressed CD81 and occludin, but not SR-BI and claudin-1. In contrast, iPS-Hep and Huh7 cells expressed all four receptors (Fig. 1A). HCVpv have been widely used in studies of the mechanism of HCV entry and in screens for inhibitors of HCV infection [30]. We therefore investigated HCVpv infection in iPS-Hep cells. iPS cells showed no susceptibility to HCVpv infection. In contrast, HCVpv dose-dependently infected iPS-Hep cells as well as Huh7 cells, a popular model cell line for HCV research (Fig. 1B). Treatment of the cells with IgG did not affect susceptibility of iPS-Hep or Huh7 cells to HCVpv infection, even at IgG concentrations of 1 μg/ml. In contrast, anti-CD81 antibody dose-dependently inhibited HCVpv infection of iPS-Hep and Huh7 cells, and the antibody treatment did not affect infection of VSVpv with iPS-Hep (Fig. 1C). These findings suggest that iPS-Hep cells are a useful model for HCV infection.

3.2. Replication of subgenomic HCV RNA in iPS-Hep cells

We previously developed Ad vectors containing tet-controllable and RNA pol I-driven HCV RNA subgenomic replicons (AdP$_I$235-HCV [replication competent], and AdP$_I$235-ΔGDD [replication incompetent]). The replicons encoded luciferase, and monitoring of luciferase activity in infected cells was a simple and convenient method to evaluate HCV replication [24]. Here, we found cells transduced with the replication-competent HCV replicon expressed luciferase in iPS-Hep cells, but not in iPS cells (Fig. 2A). In contrast, cells transduced with the replication-incompetent HCV replicon did not express luciferase (Fig. 2A). Taken together, these results suggest that replication of the HCV RNA genome occurred in the iPS-Hep cells. To confirm replication of the HCV genome, we investigated production of minus-strand HCV RNA from the positive-strand HCV RNA genome by performing real time-PCR analysis. The results of this analysis showed that minus-strand HCV RNA was produced in iPS-Hep cells and Huh7 cells, but not in iPS cells (Fig. 2B). To investigate whether the iPS-Hep cells could be used to screen for drugs that suppress HCV replication, we treated the cells with a suppressor of HCV replication, IFN. Treatment with IFN resulted in dose-dependent attenuated replication of the HCV genome with no cytotoxicity (Fig. 3A and B). These findings suggest that the iPS-Hep cells are a suitable system to use for monitoring the replication of the HCV RNA genome.

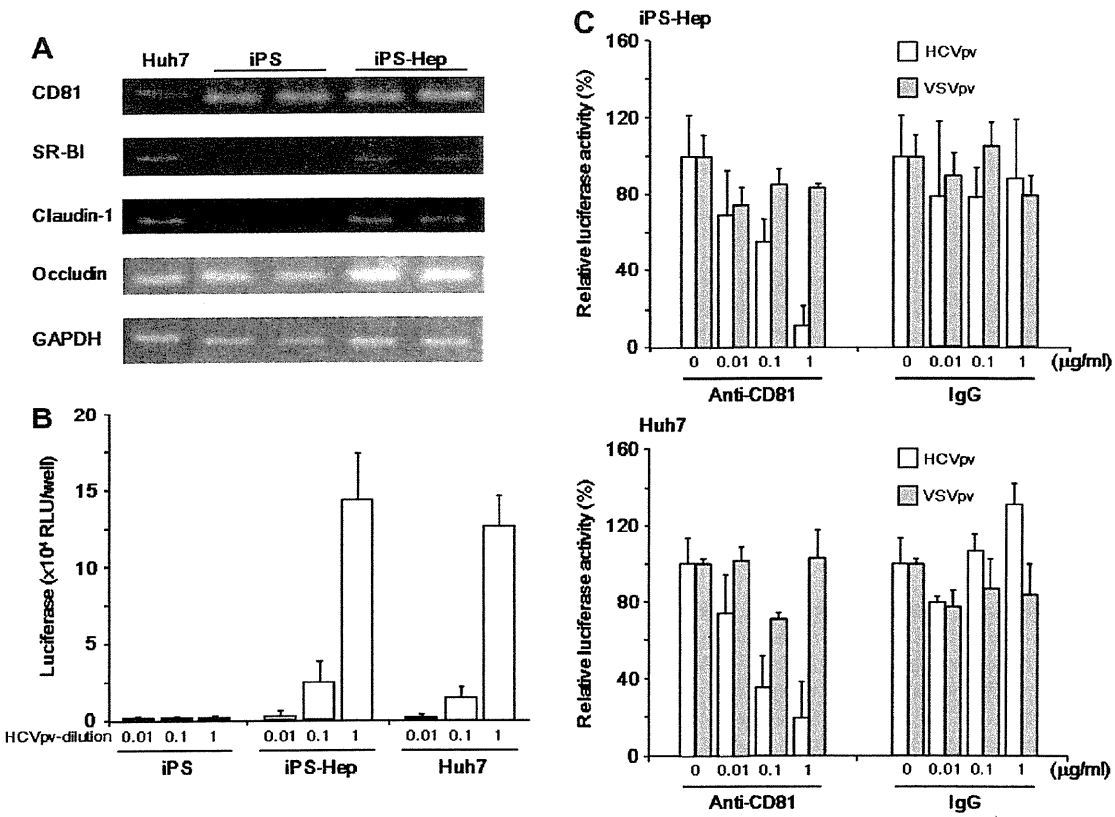

Fig. 1. HCV infection assay in iPS-Hep cells. (A) Expression of HCV receptors in iPS-Hep cells. Total RNA samples from Huh7, iPS, and iPS-Hep cells were subjected to RT-PCR analysis as described in the Section 2. The PCR products were separated on 2% agarose gels, followed by staining with ethidium bromide. (B) Infection of iPS-Hep cells with HCVpv. iPS, iPS-Hep and Huh7 cells were infected with HCVpv at the indicated dilution. After 2 h of infection, the cells were cultured with fresh medium for 24 h. Then, luciferase activities were measured. Data are presented as means ± SD ($n = 3$). (C) Effect of anti-CD81 antibody on infection of iPS-Hep cells with HCVpv. iPS-Hep (upper panel) and Huh7 (lower panel) cells were treated with mixtures of HCVpv (open column) or VSVpv (gray column) and anti-CD81 antibody or control mouse IgG at the indicated concentrations. After a 2-h incubation, the cells were cultured with fresh medium for 24 h. Then, the luciferase activities were measured. Data represent the percentage of vehicle-treated cells. Data are presented as means ± SD ($n = 3$).